An animated tectonic reconstruction of southwestern North America since 36 Ma

Nadine McQuarrie*
Brian P. Wernicke
Division of Geological and Planetary Sciences, MS 100-23, California Institute of Technology, Pasadena, California 91125, USA

ABSTRACT

We present tectonic reconstructions and an accompanying animation of deformation across the North America–Pacific plate boundary since 36 Ma. Intraplate deformation of southwestern North America was obtained through synthesis of kinematic data (amount, timing, and direction of displacement) along three main transects through the northern (40°N), central (36°N–37°N), and southern (34°N) portions of the Basin and Range province. We combined these transects with first-order plate boundary constraints from the San Andreas fault and other areas west of the Basin and Range. Extension and strike-slip deformation in all areas were sequentially restored over 2 m.y. (0–18 Ma) to 6 m.y. (18–36 Ma) time intervals using a script written for the ArcGIS program. Regions where the kinematics are known constrain adjacent areas where the kinematics are not well defined. The process of sequential restoration highlighted misalignments, overlaps, or large gaps in each incremental step, particularly in the areas between data transects, which remain problematic. Hence, the value of the reconstructions lies primarily in highlighting questions that might not otherwise be recognized, and thus they should be viewed more as a tool for investigation than as a final product.

The new sequential reconstructions show that compatible slip along the entire north-south extent of the inland right-lateral shear zone from the Gulf of California to the northern Walker Lane is supported by available data and that the east limit of active shear has migrated westward with respect to North America since ca. 10 Ma. The reconstructions also highlight new problems regarding strain-compatible extension east and west of the Sierra Nevada–Great Valley block and strain-compatible deformation between southern Arizona and the Mexican Basin and Range. Our results show ~235 km of extension oriented ~N78°W in both the northern (50% extension) and central (200% extension) parts of the Basin and Range. Following the initiation of east-west to southwest-northeast extension at 15–25 Ma (depending on longitude), a significant portion of right-lateral shear associated with the growing Pacific–North America transform jumped into the continent at 10–12 Ma, totaling ~100 km oriented N25°W, for an average of ~1 cm/yr since that time.

Keywords: Basin and Range, kinematic reconstruction, extension, plate tectonics, velocity field.

INTRODUCTION

The large-scale horizontal velocity field at Earth's surface is one of the main predictions of physical models of lithospheric deformation (e.g., England and McKenzie, 1982). Two-dimensional, cross-sectional models of finite deformation of mountain belts incorporating strong heterogeneity in rheologic parameters have been developed over the last decade (e.g., Lavier and Buck, 2002; Braun and Pauselli, 2004). Owing to advances in computation, fully three-dimensional models of plate boundary deformation zones, incorporating both horizontal and vertical variations in lithospheric rheology, will soon become common. Thus, a key observational frontier will be the determination of precise displacement vector fields of continental deformation in order to test these models. The most dramatic recent improvement in obtaining such velocity fields has been the advent of space-based tectonic geodesy (especially using continuous global positioning systems [GPS]), which is yielding velocity fields that are unprecedented in terms of both the scale of observation and the accuracy of the velocities. These data have already been used as tests for physical models in southwestern North America (e.g., Bennett et al., 1999, 2003; Flesch et al., 2000) and elsewhere (e.g., Holt et al., 2000). Substantial progress has also occurred over the last decade in determining longer-term velocity fields using the methods of plate tectonics and regional structural geology.

These longer-term displacement histories are essential for addressing the question of how the lithosphere responds to major variations in plate geometry and kinematics (e.g., Houseman and England, 1986; England and Houseman, 1986; Bird, 1998) because such variations occur on the million-year time scale. Plate tectonics is a precise method for constraining the overall horizontal kinematics of plate boundaries, using seafloor topographic and magnetic data in concert with the geomagnetic time scale. For the diffuse deformation that characterizes the continental lithosphere along plate boundaries, however, tectonic reconstruction at scales in the 100 km to 1000 km range is not as straightforward. It is based primarily on structural geology and paleomagnetic studies and requires the identification of large-scale strain markers and consideration of plate tectonic constraints (e.g., Wernicke et al., 1988; Snow and Wernicke, 2000; McQuarrie et al., 2003). Regional strain markers within the continents may not exist in any given region, and even if they do, they may not be amenable to accurate reconstruction at large scales.

*Current address: Department of Geosciences, Guyot Hall, Princeton University, Princeton, New Jersey 08544, USA.

Geosphere; December 2005; v. 1; no. 3; p. 147–172; doi: 10.1130/GES00016.1; 11 figures; 6 tables, 1 animation.

In southwestern North America, a zone of plate boundary deformation on the order of 1000 km wide is developed along the plate boundary. In mid-Tertiary time (36 Ma), this boundary was strongly convergent, with the Farallon plate subducting eastward beneath the North American plate. Beginning at ca. 30 Ma, the Pacific-Farallon ridge came in contact with the North American plate. Since then, the Pacific–North America boundary has grown through the migration of triple junctions along the coast. Now, the entire margin from southern Baja California to Cape Mendocino is a transform Pacific–North America boundary, rather than a convergent Farallon–North America boundary (Atwater, 1970). This change in the configuration of the plate boundary is both relatively simple and profound, making southwestern North America an ideal laboratory for investigating how continental lithosphere responds to changes in relative plate motion.

Refined plate tectonic reconstructions have provided an improved kinematic model of the change from convergent to transform motion and have shown that there were significant variations in the obliquity of the transform after it developed. In particular, during the interval ca. 16 to ca. 8 Ma, Pacific–North America motion was highly oblique and included a margin-normal extensional component of as much as 2 cm/yr, coeval with a rapid pulse of Miocene extension that formed the Basin and Range province (Atwater and Stock, 1998; Wernicke and Snow, 1998). At ca. 8 Ma, Pacific–North America motion changed to more purely coastwise motion, which appears to have changed the intraplate tectonic regime from profound extension to a more complex mixture of extension, shortening, and transform motion, responsible for the opening of the Gulf of California, thrust faulting of the western Transverse Ranges, and development of the San Andreas fault–eastern California shear zone–Walker Lane, respectively.

Over the last several years, high-quality, large-scale kinematic constraints, many of which resulted from decades of field work and attending debate, have become available, reaching the point where synthesis into a large-scale velocity field is feasible. A rudimentary kinematic model using many of the constraints along the plate boundary and in the plate interior was incorporated into a publicly available animation of the post–38 Ma evolution of the entire Pacific–Farallon–North America system (Atwater and Stock, 1998; animation available at http://emvc.geol.ucsb.edu/download/nepac.php).

In this paper, we synthesize the current state of information on the kinematics of the diffusely deforming North American plate since 36 Ma, based on offsets of regional structural markers, and construct a strain-compatible kinematic model of the horizontal motions at 2 m.y. (0–18 Ma) and 6 m.y. (18–36 Ma) intervals, presented as a continuous animation. The model is by no means a final product, as new kinematic information and testing will require significant modifications of the model. Rather, the model is an attempt to be quantitatively rigorous in a way that will be useful for comparison with large-scale, three-dimensional physical models and for the identification of issues regarding the structural kinematics that might not otherwise be detected. Thus, in addition to the animation, we have constructed ''instantaneous'' velocity fields based on 2 m.y. averages from 0 Ma to 18 Ma and 6 m.y. averages from 18 Ma to 36 Ma. These results are our best attempt at ''paleogeodesy,'' presenting the geology-based kinematic model in a format similar to modern GPS velocity fields, which in turn may be quantitatively compared to physically based model velocity fields.

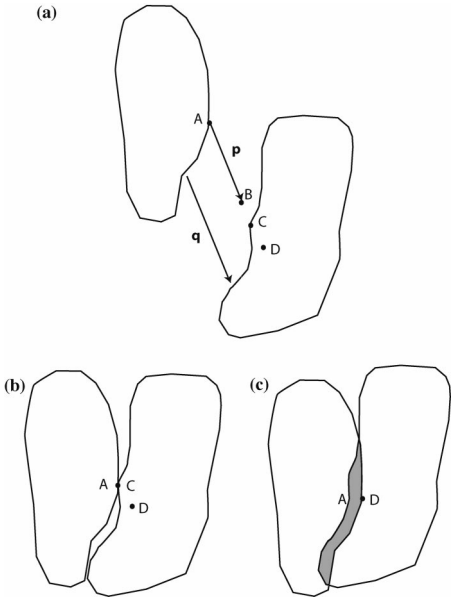

Figure 1. Schematic diagram illustrating the method of using regional structural constraints to limit possible displacement paths in tectonic reconstructions. See text for discussion and explanation of letters.

METHODS

By combining regional structural constraints into a single model, the self-consistency of the model (i.e., its strain compatibility through time) provides powerful additional constraints on the kinematics in at least three ways. The first and most important is the fact that high-quality local kinematic information imposes severe constraints on its surroundings where information may not be available. As a hypothetical example, consider a large region of oblique extension between two undeformed blocks (Fig. 1). The strain and strain path need not be known for each geological element in the deforming region in order to constrain the large-scale kinematics. If the sum of fault displacements across just a single reconstruction path (**p)** is known, restoring point A to a position at point B, and it is known that the blocks have not rotated, then the single path imposes a strong constraint on the overall kinematics of all of the other paths between the blocks (Fig. 1A).

The second additional constraint is on errors in reconstructions. In the example in Figure 1, let us suppose that the minimum value of all fault displacements along reconstruction path **p** restores the block to point B, but there is no constraint on the maximum value along the path itself. The side of the block containing A would overlap the block on the other side of the rift if the displacement along the path were in excess of AC (Fig. 1B), violating the condition of strain compatibility. Therefore, the displacement is constrained to be between AB and AC, rather than some value greater than AB.

A third and perhaps most useful additional constraint arises when local constraints contradict one another. For example, if reconstruction along path **q** (Fig. 1A) required that point A restore to a position D, which is well within the other block, then the violation of strain compatibility forces reevaluation of the geological constraints. The geological reconstruction for displacement along **q,** the paleomagnetic constraints on the blocks, and the presumed rigidity of the blocks cannot all be correct. Thus, the exercise of regional reconstruction focuses attention on information that is most critical for improving the accuracy of the reconstruction. For southwestern North America, there is now enough high-quality local kinematic information that large-scale self-consistency of the model imposes useful additional constraints in all of these ways.

In making the reconstruction, the methods used in the local study of Wernicke et al. (1988) and Snow and Wernicke (2000) in the Death Valley region of the central Basin and Range province were applied at large scale. In Snow and Wernicke (2000), each step in the reconstruction showed the paleoposition of existing mountain ranges. Although the recon-

struction allowed for the ranges to change shape as extension is restored (i.e., the ranges may decrease in area), in our reconstruction, the mountain ranges are shown as digitized polygons that approximate: (1) the modern bedrock-alluvium contact (e.g., a typical range in the Basin and Range), (2) faults bounding individual crustal blocks (e.g., the Santa Ynez Mountains block in the western Transverse Ranges), or (3) the physiographic boundaries of large, intact crustal blocks (e.g., the Colorado Plateau). In some cases, especially where large extensional strains are involved, the reconstruction overlaps individual polygons to account for extension, essentially using the modern bedrock-alluvium contact as a geographical reference marker. Because the strain is extensional, and in the case of metamorphic core complexes, one range has literally moved off of the top of another, these overlaps do not violate strain compatibility.

The individual positions of polygons were restored in each 2 m.y. time frame through an ArcGIS script that reads and updates a table listing the kinematic data for each range. The script, created by Melissa Brenneman of the Redlands Institute at the University of Redlands, is written in Visual Basic and is incorporated as a tool in a custom ArcMap document. The script reads a dBASE 4 table that contains the movement parameters (direction, distance rotation, and time interval) for each range (Appendix 1).[1] The movement parameters listed in the table include both the available data (Figs. 2–5), as well as the motion required for strain compatibility. For the regions where kinematic data are not available, the kinematics could be defined by inserting data from proximal areas, or individual ranges could be moved by hand with the motion updated and recorded in the dBASE table using the ArcGIS script. The ArcGIS format and accompanying script allows for exact displacements to be incorporated into the model, as well as the individual adjustment of ranges to ensure strain compatibility. The GIS script records the geographical position of the centroid of each range at each 2 m.y. or 6 m.y. epoch. This allows for the data to be displayed in a variety of ways, including palinspastic maps for each 2 m.y. or 6 m.y. epoch, instantaneous velocity vectors at each 2 m.y. or 6 m.y. epoch, ''paths'' that individual ranges take over the 36 m.y. span of the reconstruction, or an animation that shows the integrated motion over 36 m.y. Instantaneous geology velocity fields are obtained from connecting the centroids of specific ranges at one time with the centroid of the same range in a later time.

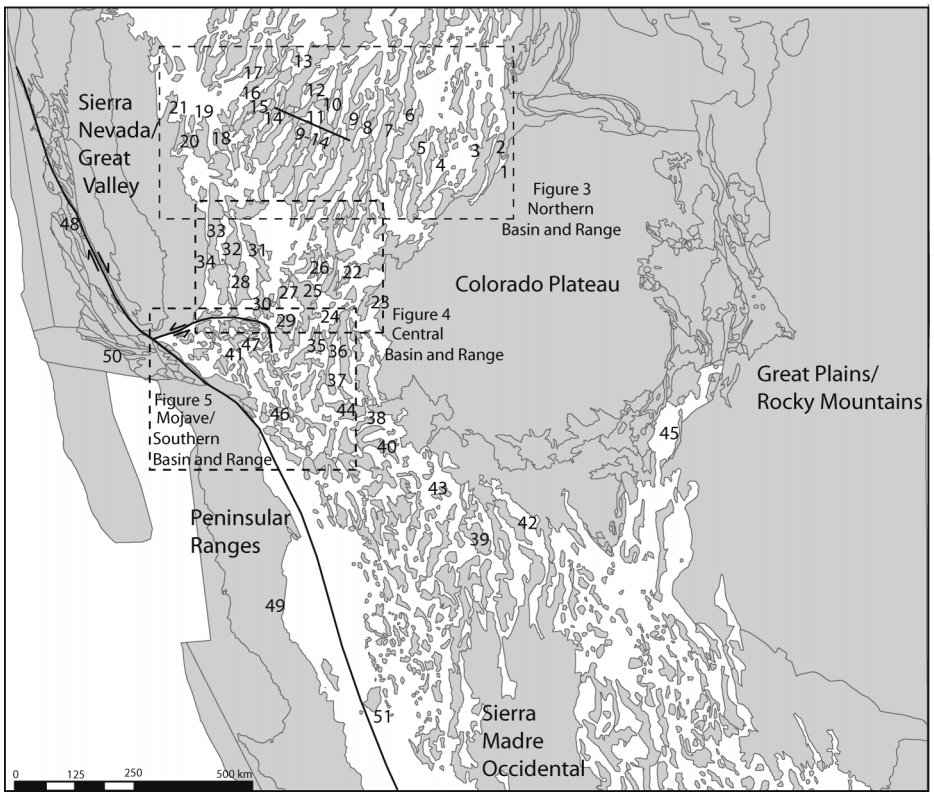

Figure 2. Map of western North America showing the primary tectonic elements in the reconstruction. The gray shaded polygons represent the physiographic or geologic expression of mountain ranges, which in the Basin and Range are fault bounded and separated by alluvial valleys. Dashed boxes are the locations of Figures 3–5. The numbers refer to specific mountain ranges identified in Tables 1–6.

DATA

The primary tectonic elements in the reconstruction are large crustal blocks comprising flat-lying pre–36 Ma strata, or geologic elements that are otherwise little deformed, and the straining areas in between them. The large unstrained blocks include the Great Plains–Rocky Mountains region (nominal North America reference frame), the Sierra Madre Occidental, the Colorado Plateau, the Sierra Nevada–Great Valley block, and Peninsular Ranges block (Fig. 2). The strained areas around them include the Rio Grande rift and Basin and Range province, the Gulf of California, the Transverse Ranges, the Coast Ranges, and the Continental Borderlands province offshore of southern California and Baja California.

The constraints used in the reconstruction are organized into six major categories (Tables 1–6). The first covers a range-by-range reconstruction path across the northern Basin and Range near latitude 40°N (Fig. 3 and Table 1). The second includes a similar reconstruction path across the central Basin and Range near latitude 37°N (Fig. 4 and Table 2). These two reconstructions collectively constrain the motion of the Sierra Nevada–Great Valley block. The third includes constraints from the southern Basin and Range, mainly the mid-Tertiary metamorphic core complexes of the Colorado River corridor and southern Arizona, west of the Sierra Madre Occidental, and extension across the Rio Grande rift north and east of the Sierra Madre Occidental (Table 3). The fourth includes the complex Oligocene to recent strike-slip and extensional displacements of the Mojave region, which connect the Sierran displacement to regions farther south (Fig. 5 and Table 4). The fifth includes paleomagnetic and geologic constraints on vertical axis rotations of large crustal blocks, including the Sierra Nevada and Colorado Plateau, as well as small, individual ranges within the

[1]GSA Data Repository item 2005200, Appendix 1, Movement Table, paleogeographic maps, and ArcGIS files (shape files for each reconstructed time step), is available online at www.geosociety.org/pubs/ft2005.htm, or on request from editing@geosociety.org or Documents Secretary, GSA, P.O. Box 9140, Boulder, CO 80301-9140, USA

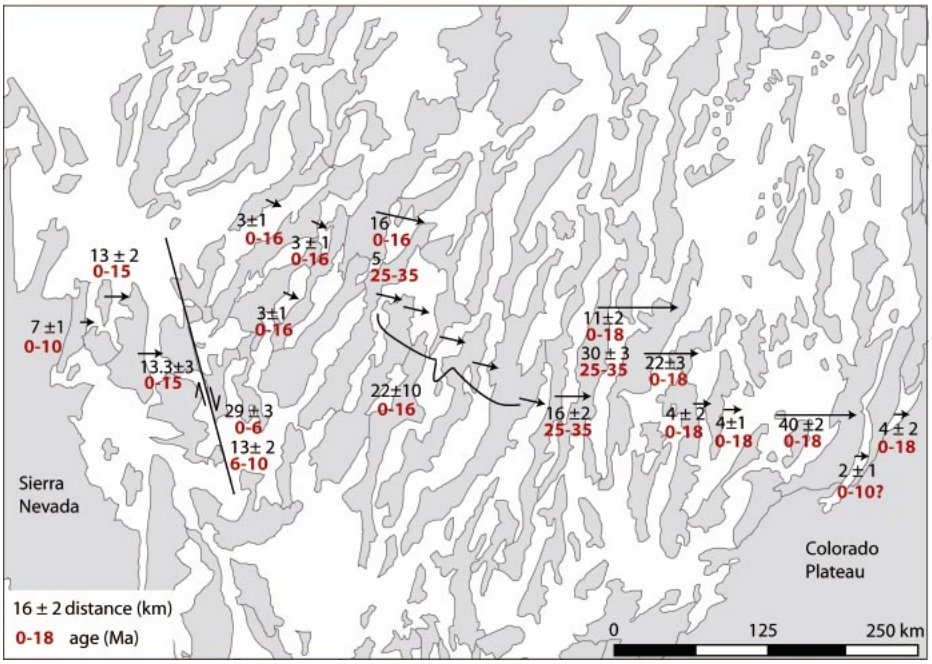

Figure 3. Map of the northern Basin and Range showing the kinematic data incorporated into the model. Black numbers indicate horizontal displacement amount, red bold numbers indicate age range of motion. Arrows indicate approximate magnitude and direction of individual relative displacements between polygons. Data compiled from Allmendinger et al., 1986; Armstrong et al., 2004; Bartley and Wernicke, 1984; Coogan and DeCelles, 1996; DeCelles et al., 1995; Dilles and Gans, 1995; Faulds et al., 2003; Hardyman et al., 1984; Hintzi, 1973; Hudson and Oriel, 1979; Lee, 1999; Miller et al., 1999; Niemi, 2002; Niemi et al., 2004; Smith, 1992; Smith et al., 1990; Smith and Bruhn, 1984; Stockli, 2000, 2001; Surpless, 1999.

central Basin and Range and Mojave regions (Table 5). Lastly, constraints on the large displacements along the San Andreas fault–Gulf of California shear system, and strains and rotations within the Continental Borderlands, including the large clockwise rotation of the Santa Ynez Mountains block, are included in Figure 6 and Table 6.

Northern Basin and Range

The extensional kinematics of the northern Basin and Range are dominated by two large-offset normal fault systems, the Snake Range detachment system (78 km of total offset) and the Sevier Desert detachment (40 km of total offset). The Snake Range detachment system affects the Egan, Schell Creek, and Snake Ranges (Fig. 2, ranges 6–8). Although the coupling of this system of faults to deep crustal extension has been debated (e.g., Gans and Miller, 1983; Miller et al., 1983; Bartley and Wernicke, 1984; Miller at al., 1999; Lewis et al., 1999), a magnitude of upper crustal extension of 78 km ± 10 km, as determined through mapped and restored stratigraphic markers, is not controversial (Gans and Miller, 1983; Bartley and Wernicke, 1984). More controversial is the geometry of the extensional faults in the Sevier Desert basin (between ranges 3 and 4, Fig. 2), including the very existence of the Sevier Desert detachment, which is known only from interpretations of seismic reflection profiles and well data (Anders and Christie-Blick, 1994; Wills et al., 2005). The 40-km offset along the Sevier Desert detachment used in this paper is based on restoring Sevier fold-thrust belt structures that are offset by the detachment, and high-angle normal faults in the hanging wall imaged in the Consortium for Continental Reflection Profiling (COCORP) and industry seismic reflection lines (Allmendinger et al., 1986; Allmendinger et al., 1995; Coogan and DeCelles, 1996). An opposing view to the large-offset kinematics of a shallow detachment suggests that the imaged reflection surface is a composite of aligned features that includes basin-bounding high-angle normal faults, a subhorizontal thrust fault, and an evaporite horizon (Anders and Christie-Blick, 1994). According to this interpretation, extension across ranges within and around the Sevier Desert basin could be as little as 10 km (versus 40 km), which would subtract ~15% from our overall estimate of extension along the transect.

To the west of the Egan Range area, the remainder of the northern Basin and Range deformation is partitioned into extensional and right-lateral strike-slip offsets, both of which accommodate translation of the Sierra–Great Valley block away from the interior of North America. The extension (94 km) is accommodated by several systems of steeply tilted normal fault blocks in the western Basin and Range, with individual fault systems accommodating up to 16 km of extension (Fig. 2, ranges 13, 19, and 20) (Surpless, 1999; Dilles and Gans, 1995; Smith, 1992), and a number of high-angle, presumably modest-offset normal faults that define the Basin and Range physiography across the central part of the reconstruction path, which we assume have 3–4 km of horizontal offset each.

Right-lateral shear is accommodated predominantly through northwest-trending faults concentrated near the western edge of the northern Basin and Range in the northern Walker Lane Belt (Fig. 2, range 18). Right-lateral offset on a series of faults, which individually have 5–15 km of offset, totals 20–56 km (Faulds et al., 2005; Hardyman et al., 1984). Because the faults strike more westerly than the North American margin, their motion accommodates a component of westward motion of the plate boundary.

Timing of extension in the northern Basin and Range is constrained by a large body of work on the ages of faulted Cenozoic volcanic and sedimentary units and cooling ages of uplifted footwall blocks. For example, the early ''core complex''–related extension (ca. 35–25 Ma) is seen in coeval faulting and volcanism at 35 Ma in the Egan Range (Gans and Miller, 1983) and $^{40}Ar/^{39}Ar$ cooling ages indicative of rapid cooling from 30 to 25 Ma in the western portion of the northern Snake Range and from 20 to 15 Ma in the eastern portion of the range (Lee, 1995). Apatite fission track (AFT) cooling ages from the northern Snake Range indicate 10–13 km of fault slip from 18 to 14 Ma. Initiation of later ''Basin and Range'' extension is seen predominantly in the fission-track and helium cooling ages of apatite and zircon. The cooling ages across the width of the extending zone cluster ca. 15 Ma (Stockli, 1999), with 18 Ma ages in the footwall of the Snake Range detachment (Miller et al., 1999) (Fig. 2, range 6) and Sevier Desert detachment (Stockli et al., 2001) (Canyon Range, Figure 2, range 3).

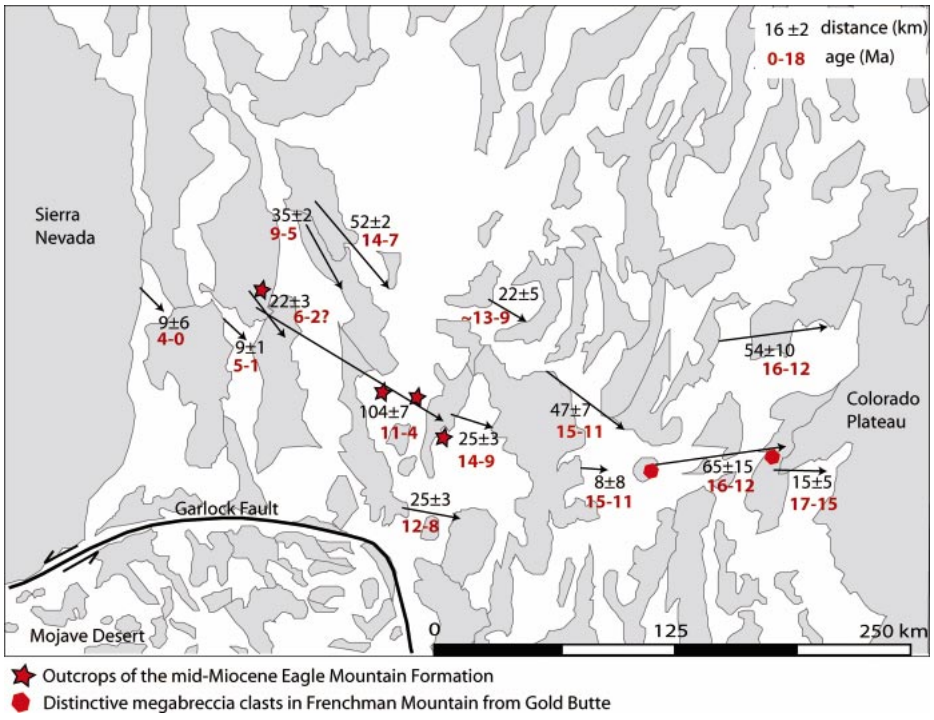

Figure 4. Map of the central Basin and Range showing the kinematic data incorporated into the model. Motion of the Sierra Nevada with respect to the Colorado Plateau in this region is predominantly constrained by two distinctive sedimentary deposits (indicated as stars and hexagons) offset along extensive normal and strike-slip fault systems. Arrows indicate approximate magnitude and direction of individual relative displacements between polygons. Black numbers indicate horizontal displacement amount, bold red numbers indicate age range of displacement. Data from Axen et al., 1990; Brady et al., 2000; Burchfiel, 1968; Burchfiel et al., 1987; Cemen et al., 1985; Duebendorfer et al., 1998; Fitzgerald et al., 1991; Fowler and Calzia, 1999; Guth, 1989; Holm and Dokka, 1991, 1993; Hoisch and Simpson, 1993; Niemi et al., 2001; Snow and Lux, 1999; Snow and Wernicke, 1989, 2000; and Wernicke et al., 1988.

Central Basin and Range

The central Basin and Range province is in many respects an ideal location for a province-wide restoration of Basin and Range extension (Snow and Wernicke, 2000, and references therein). A regionally conformable miogeocline, Mesozoic thrust structures and distinctive Tertiary sedimentary deposits tightly limit the extensional history of both the Lake Mead (Fig. 2, ranges 22–25) and the Death Valley (Fig. 2, ranges 27–34) extensional systems (Wernicke et al., 1988; Wernicke, 1992). Motion of the Sierra Nevada with respect to the Colorado Plateau in this region is primarily constrained by displacements of two distinctive Miocene basins developed early in the history of the extension of each system (Fig. 4).

In the Lake Mead system, restoring numerous proximal landslide breccias at Frenchman Mountain (Fig. 2, range 24) to their source areas in the Gold Butte block (Fig. 2, range 23) also restores piercing lines defined by the southward truncation of Triassic formational boundaries by the basal Tertiary unconformity in both areas. The correlation of these features in the Frenchman Mountain and Gold Butte areas suggests 65 km ± 15 km of extension between the two blocks (Fig. 4).

In the Death Valley system, Wernicke et al. (1988) initially proposed that the Panamint thrust at Tucki Mountain (Panamint Range, Figure 2, range 28) is correlative with the Chicago Pass thrust in the Nopah–Resting Springs Range (Fig. 2, range 27) and the Wheeler Pass thrust in the Spring Mountains (Fig. 2, range 25), suggesting a total of 125 km ± 7 km of post-Cretaceous, west-northwestern extension has separated them (Table 2). This offset is strengthened by correlations of additional contractile structures exposed across the Death Valley extensional system (Snow and Wernicke, 1989; Snow, 1992; Snow and Wernicke, 2000) and distinctive middle Miocene sedimentary deposits that occur along the extensional path (Niemi et al., 2001). These include proximal conglomeratic strata of the Eagle Mountain Formation, which were derived from the northeastern margin of the Hunter Mountain batholith in the southern Cottonwood Mountains (Fig. 2, range 32). Recognition and correlation of this dismembered early extensional basin, in conjunction with stratigraphic constraints from other Tertiary deposits in the region, indicates that its fragmentation occurred mainly from 12 Ma to 2 Ma (Fig. 4). The correlation of these deposits yields a displacement vector of 104 km ± 7 km oriented N67°W between the Nopah–Resting Springs Range (Fig. 2, range 27) and the Cottonwood Mountains (Fig. 2, range 32).

To the ~170 km of displacement from these constraints, we add four additional estimates to complete the reconstruction path. In the Lake Mead system, 15 km of extension between the Gold Butte area and the Colorado Plateau (Fig. 2, range 23) (Brady et al., 2000) and a maximum of 8 km of extension between the Spring Mountains (Fig. 2, range 25) and Frenchman Mountain (Fig. 2, range 24) (Wernicke et al., 1988) increases the total displacement of the Spring Mountains relative to the Colorado Plateau to ~88 km. In the Death Valley system, an addition of 9 km of displacement in both the Panamint and Owens Valleys increases the total displacement to ~147 km between the Spring Mountains and the Sierra Nevada.

The sum of all displacements along the path is therefore 235 km ± 20 km (Table 2), which represents a combination of areal dilation (crustal thinning) and plane strain (strike-slip faulting). Approximately 80% of the elongation is accommodated by vertical thinning and ~20% by north-south contraction (Wernicke et al., 1988; Snow and Wernicke, 2000). In addition to this path, there are a number of more local offsets that were used to position polygons to the north and south, which are shown in Figure 4 and summarized in Table 2.

Southern Basin and Range–Rio Grande Rift

Extension in the southern Basin and Range is almost completely dominated by the formation of large-offset normal faults that form the metamorphic core complexes (Coney, 1980; Spencer and Reynolds, 1989; Dickinson, 2002). The core complexes ring the southwestern margin of the Colorado Plateau (Fig. 2, ranges 37–44), and estimates of the

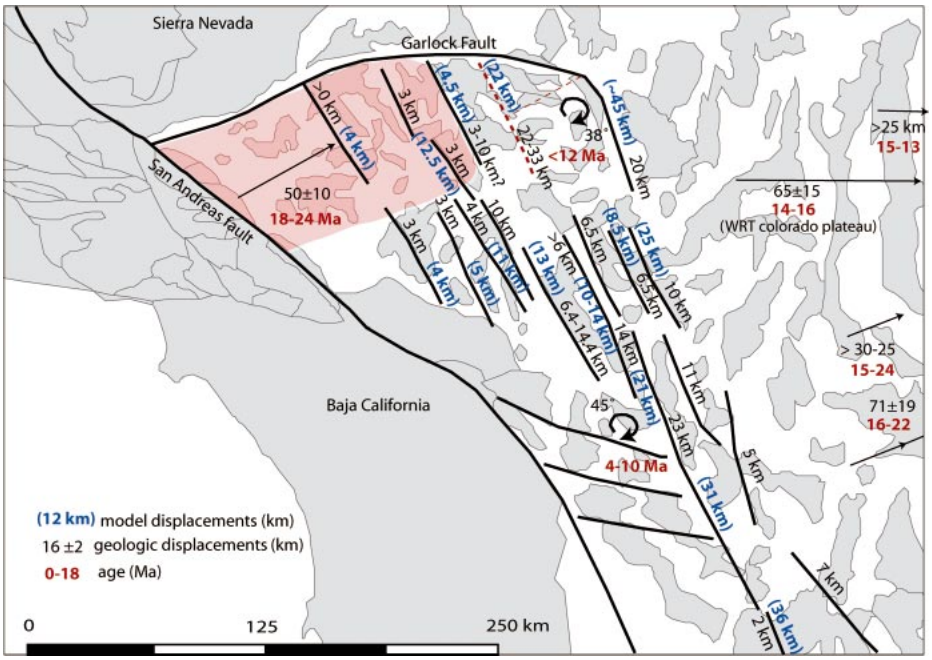

Figure 5. Map of the Mojave and Southern Basin and Range region showing distribution of strike-slip faults (bold lines), vertical axis rotation data (curved arrows), and extensional offsets (straight arrows). For strike-slip faults, reported slip amounts (black numbers) are contrasted with model slip (bold blue numbers). For extension and rotation constraints, black numbers indicate horizontal displacement or amount of rotation, bold red numbers indicate age range of deformation. Red shaded area is the area of the model that undergoes 24–18 Ma core complex extension in the Mojave region. WRT indicates measured displacement is "with respect to" the Colorado Plateau. Data from Ballard, 1990; Bassett and Kupfer, 1964; Dokka, 1983, 1989; Foster et al., 1993; John and Foster, 1993; Hamilton, 1987; Howard and Miller, 1992; Miller, 1980; Miller and Morton, 1980; Powell, 1981; Richard et al., 1992; Richard, 1993; Richard and Dokka, 1992; Spencer and Reynolds, 1989; Spencer et al., 1995; Schermer et al., 1996; Walker et al., 1995.

total extension they represent are remarkably systematic in magnitude, direction, and rate (Table 3). The timing of extension varies in age from 28 Ma to 14 Ma as the extension migrates from southeast to northwest. The migration of extension has been related to a similar migration in volcanism. Both extension and volcanism have been proposed to be a result of the northwestward foundering of the Farallon plate (e.g., Humphreys, 1995; Dickinson, 2002).

In a similar time frame (ca. 26 Ma), volcaniclastic sediments deposited east of the Colorado Plateau in the Rio Grand Rift (Fig. 2, location 45) have been interpreted as representing the onset of extension (Chapin and Cather, 1994). Ingersoll (2001) counters that the early sediments are broad volcaniclastic aprons that show no evidence of syndepositional faulting. He places the initiation of rifting slightly later (ca. 21 Ma). Based on initiation of half-graben sedimentation and stratal tilting, rapid extension occurred between 17 and 10 Ma (Ingersoll, 2001; Chapin and Cather, 1994). The total magnitude of extension is small and ranges from 6 km in the northern part of the rift to 17 km in the south, consistent with the 1.5° clockwise rotation of the Colorado Plateau (Chapin and Cather, 1994; Russell and Snelson, 1994).

Extension within the Rio Grande rift is contiguous with the broad extended region farther south, east of the Sierra Madre Occidental (in Chihuahua), the magnitude of which is poorly understood (Dickinson, 2002). Generally, extension in the Mexican Basin and Range is partitioned both in time and space. Early core complex extension is documented in northwestern Mexico (in Sonora), just west of the Sierra Madre Occidental (Nourse et al., 1994; Gans, 1997) (Fig. 2). Palinspastic reconstructions over small regions in Sonora suggest cumulative extension of 90%, mostly between 26 and 20 Ma, and more modest extension (10%–15%) between 20 and 17 Ma (Gans, 1997). Limited crustal extension is also documented east of the Sierra Madre Occidental during the same time period (Dickinson, 2002). Major extension occurred in both Chihuahua (Henry and Aranda-Gomez, 2000; Dickinson, 2002) and Sonora Mexico (e.g., Stock and Hodges, 1989; Henry, 1989; Lee et al., 1996) from ca. 12 Ma to 6 Ma as a prelude to the opening of the Gulf of California at 6 Ma (Oskin et al., 2001). During the 12 Ma to 6 Ma interval, very small magnitude east-west "Basin and Range" extension affected Arizona (Spencer and Reynolds, 1989; Spencer et al., 1995).

Mojave Region

Cenozoic deformation of the Mojave region occurred in two main stages. Deformation began in the late Oligocene–early Miocene with the formation of large-offset normal faults and associated core complexes (Glazner et al., 1989; Dokka, 1989; Walker et al., 1990). Extension in the Mojave region (Fig. 2, location 41, and Fig. 5) may be linked to core complex extension in the southern Basin and Range corridor (Fig. 2, ranges 38 and 44) through a diffuse transfer zone that involves both rotation and strike-slip faulting (Bartley and Glazner, 1991; Martin et al., 1993). The magnitude of extension is determined through alignment of pre-extensional markers that include facies trends in Paleozoic strata, a unique gabbro-granite complex, and late Jurassic dikes, indicating a total of 40–70 km of offset (Glazner et al., 1989; Walker et al., 1990; Martin et al., 1993). Extension began in synchronism with the eruption and emplacement of 24–23 Ma igneous rocks (Walker et al., 1995) and is capped by the flat-lying, 18.5 Ma Peach Springs Tuff (Glazner et al., 2002). The fraction of the Mojave Desert region that was affected by mid-Tertiary extension is controversial (e.g., Dokka, 1989; Glazner et al., 2002). Glazner et al. (2002) propose that only a small region north of Barstow (Fig. 2, location 41) was affected by the early extension, with the southern boundary of this extensional domain linked to core complex extension to the southeast through diffuse right-lateral shear. The northern boundary of the extensional domain is more problematic; however, regional kinematic compatibility requires a northern transfer zone that links Mojave extension to similar age extension to the north or west. Rotation of the Tehachapi Mountains and/or extension in the southern San Joaquin Valley may represent the northern portion of this system (McWilliams and Li, 1985; Plescia and Calderone, 1986; Tennyson, 1989; Goodman and

TABLE 1. DATA USED FOR RESTORING EXTENSION IN NORTHERN BASIN AND BASIN AND RANGE LATITUDE 40° N

Range/fault	Horizontal displacement of range block (model polygon)	Horizontal component of fault slip (data)	Timing of slip	Rate of deformation (horizontal component of fault slip/duration)	Direction of motion	Data used	Source	Cumulative path displacement (± cumulative error)	Long. (x)	Lat. (y)
San Pitch/Gunnison (1) [346]	4 km	4 km ± 2	~18–0 Ma	0.22 km/m.y.	E-W	Stratigraphic separation	Hintze, 1973	4 km ± 2 km	−111.78879	39.50297
Canyon/Levan and Fayette segments, Wasatch fault (2) [358]	5 km	5 km ± 2 km	~10–0 Ma	0.5 km/m.y.	E-W	Holocene vertical offset rates and Miocene exhumation rates, assume ~30° dip	Neimi et al., 2004; Machette et al., 1992; Jackson, 1991; Smith and Bruhn, 1984;	6 km ± 3 km	−112.15421	39.56062
Cricket Range/Sevier Desert Detachment (3) [300]	34 km	40 km ± 2 km	~18–0 Ma	2.22 km/m.y. (total)	E-W	Matching CR culmination in surface and subsurface.	Coogan and DeCelles, 1996; Coogan et al., 1995	46 km ± 3.5 km	−112.75582	39.21301
	12 km	12-10 km	~19–15 Ma	3 km/m.y.		AFT cooling ages assuming a 34-40 degree fault	Stockli et al., 2001			
	22 km	16-30 km	15–0 Ma	1 km/m.y.			Stockli et al., 2001			
House Range/"Reflection F" fault (4) [350]	3.33 km	4 km ± 1 km	~15 Ma	.267 km/m.y.	E-W	Offset reflector on seismic line	Allmendinger et al., 1986	50 km ± 3.6 km	−113.34716	39.23402
Confusion Range/House Range fault (5) [359]	4.66 km	4 km (2–3 km exhumation)	~15 Ma		E-W	AFT cooling age	Stockli, 1999		−113.61446	38.88285
Snake Range/northern Snake Range decollement (6) [366]	30 km (25–35), 22 km (0–18)	30 km ± 3 km (0) 22 ± 3 km	35–25 Ma, (pause 25–18Ma) 18–0 Ma	3 km/m.y. from 35–25 Ma, 2 km/m.y. from 18-0 Ma, 3 km/m.y. from 18-14 Ma, 1.7 km/m.y. from 14-0 Ma	E-W	Map relations stratigraphic offset, Ar/Ar cooling ages and AFT data (suggests 10.5-13 km of slip between 18-14 Ma)	Gans and Miller, 1983; Bartley and Wernicke, 1984; Lee 1995; Miller et al., 1999; Lewis et al., 1999	102 km ± 5.5 km	−114.11642	39.43517
Schell Creek Range/Spring Valley fault (7) [362]	11 km (0–18)	11 km ± 2 km	18–0 Ma	1.6 km/m.y. from 35-25 Ma, 6 km/m.y. from 18-0 Ma	E-W	Map relations, AFT, ZFT, Ar/Ar	Bartley and Wernicke, 1984; Gans et al., 1985; Lee, 1995; Miller et al.,1999; Lewis et al., 1999	113 km ± 6 km	−114.63925	39.22082
Butte Mtns./Egan Range low-angle faults (8) [80]	16 km (25–35)	16 km ± 2 km, 5 km exhumation	35–25 Ma 16–17 Ma		E-W		Bartley and Wernicke, 1984; Gans et al., 1985; Lee, 1995; Stockli, 1999	129 km ± 6 km	−114.91863	39.07945
Egan Range to Shoshone Mountains (9–14)	45.6 km	47 km ± 10 km (26 excluding Toiyabe range)	16–0 Ma	26 km/16 m.y./5 ranges	E-W	Map relations and cross section restoration.	Smith et al., 1991	176 km ± 11.8 km		
Pine Range/Grant Range and Buck Range faults (9) [348]	5 km	6 km ± 1.5 km, ~5 km exhumation	~15 km	.325 km/m.y.	E-W	"	Lund et al., 1993; Taylor et al., 1989		−115.37732	40.39933
Diamond Range/Pancake Range/ Mahogany Hills faults (10) [360]	5 km	5 km of 26 total	unknown, assumed ~16–0 Ma	.325 km/m.y.	E-W	Map relations and cross section restoration.	Smith et al., 1991		−115.82060	39.83001
Sulfur Springs Range faults (11)	5 km	5 km of 26 total	assumed ~16–0	.325 km/m.y.	E-W	"	Smith et al., 1991			
Toquima Range/Simpson Park Mountains fault (12) [364]	5 km	5 km of 26 total	assumed ~16–0	.325 km/m.y.	E-W	"	Smith et al., 1991		−116.82368	39.15694
Toiyabe Range faults (13) [368]	5 km (25–35), 16 km (0–16)	21 km extension, ~5 km exhumation	35–25 Ma, 16–0 Ma	.5 km/m.y. (35-25), 1 km/m.y. (16-0)	E-W	"	Smith, 1992; Stockli, 1999	176 km ± 11.8 km	−116.81732	40.33706
Shoshone Mountain faults (14) [363]	4.6 km	5 km of 26 total	assumed ~16–0 Ma	.325 km/m.y.	N 64 W	"	Smith et al., 1991		−117.37972	39.47125
Paradise Range fault (15) [351]	3.5 km	3 km ± 1	assumed ~16–0 Ma	.188 km/m.y.	N 65 W	Paradixe, C. Alpine and Stillwater Ranges represent 100 km area that has geographical extent on map		179 km ± 11.8 km	−117.56178	39.32198
C. Alpine Range fault (16) [349]	3 km	3 km ± 1	assumed ~16–0 Ma	.188 km/m.y.	N 65 W	Extended an unknown amount		182 km ± 11.8 km	−117.70814	39.75161
Stillwater Range fault (17) [354]	1.5 km	3 km ± 1	assumed ~16–0 Ma	.188 km/m.y.	N 65 W	Unknown/best estimate		185 km ± 11.8 km	−117.85557	40.26451
Gillis/Gabbs Valley Range. Gumdrop hills, Indian head, Benton spring, Petrified Spring faults. (18) [326]	−117.85557	40.26451	younger than 25 Ma	6.75 km/m.y. (if since 8 Ma)	N 14 W	Offset of steep beds (Triassic age), granite intrusions and tuffs	Hardyman et al., 1984	203 km ± 13.3 km	−118.46915	38.81173
Northern Walker Lane fault system (18)	29 (0–6), 13 (8–10)	35 ± 5 km right lateral	younger than 25 Ma	5-10 km/m.y. (if since 5 Ma)	N 37 W	Offset segments of East trending Oligocene paleovalley	Faulds et al., 2003			
Wassak Range fault system (19) [354]	16 km	11.76 ± 1 km (13.3 ± 3 km)	15–0 Ma		E-W	Cross section restoration plus unroofing of granite	Surpless, 1999; Stockli et al., 2002	215 km ± 13.6 km	−118.88407	38.66236
	10.5 km	8.71 km	14–15 Ma	4.3 km/m.y.	E-W	from valley between Singatse	"			
	2 km	2.1 km	9–7 Ma	1.05 km/m.y.	E-W	and Wassak ranges	"			
	3.4 km	0.5 km (0 ± 2), 2.5 ± 2	7–0 Ma	.3 km/m.y.	E-W		"			
Singatse Range fault system (20) [365]	15.66 km	13 ± 2	15 to 0 Ma			Offset volcanic and sedimentary rocks, Ar/Ar isotope ages	Dilles and Gans, 1995	228 km ± 13.8 km	−119.25357	38.95920
	7.66 km	Main phase 7.26	14–12 Ma	3.63 km/m.y.	E-W		"			
	4.4 km	1.7 km	11–8 Ma	.56 km/m.y.	E-W		"			
	3.6 km	4.1 km	7–0 Ma	.58 km/m.y.	E-W		"			
Buckskin Mtns./Pine Nut Valley/Pine Nut Range Faults (21) [352]	5 km	7 ± 2, 2–3 km of exhumation	10–0 Ma	.7 km/m.y.	E-W	Offset from mapped units; timing (10-5 Ma) from Surpless	Hudson and Oriel, 1979; Stockli, 1999	231 km ± 14 km	−119.45846	38.71853
Total extension	236 km	235 ± 14 km			N 78° W					

Note: Long.—longitude; Lat.—latitude. CR—Canyon Range; AFT—Apatite Fission Track cooling age. Numbers in parentheses refer to specific ranges identified on Fig. 2; numbers in brackets refer to the RANGE_ID number for individual ranges in the ArcGIS shape files and the Movement Table (ArcGIS files, Movement Table [see footnote 1]). The cumulative error reported in column 9 equals the square root of the sum of the squares for individual vectors.

TABLE 2. DATA USED FOR RESTORING EXTENSION IN CENTRAL BASIN AND RANGE LATITUDE OF 38° N

Range/fault	Horizontal displacement of range block (model polygon)	Horizontal component of fault slip (data)	Timing of slip	Rate of deformation (horizontal component of fault slip/duration)	Direction of motion	Data used	References	Cumulative displacement of fault slip data (± cumulative error)	Long. (x)	Lat. (y)
Mormon Mountains area/ Mormon Peak, Tule Springs and Castle Cliff detachments (22) [73]	68 km	54 ± 10	16–12 Ma	13.5 km/m.y.	S 60 E	Cross section reconstruction through Beaver Dam/Tule Springs and Mormon Peak detachment systems	Axen et al., 1990	54 km ± 10 km	−114.24552	37.09463
Gold Butte/South Virgin Mountains detachment (23) [57]	18 km	15 ± 5	~17–15 Ma	7.5 km/m.y.	E-W	Cross section reconstruction, AFT cooling ages, overlapping 15 Ma basalt	Wernicke et al., 1988; Brady et al., 2000; Fitzgerald et al., 1991	15 km ± 5 km	−114.20920	36.38748
Frenchman Mountain/Lake Mead fault system (24) [47]	60 km	60 min 90 max 65 ± 15	16–12 Ma	16.25 km/m.y.	N 75 E	Megabreccia from Gold Butte, pinchout of Mz formations, Virgin Mountains detachment system	Snow and Wernicke, 2000; Duebendorfer and Black, 1992; Duebendorfer et al., 1998; Wernicke et al., 1988	80 km ± 16 km	−114.96999	36.20312
Spring Mountains/Las Vegas fault system (25) [53]	8 km	8 km ± 8	15–11 Ma		N 75 E	Unknown amount of extension between Spring Mountain and Frenchman Mtn.	Wernicke et al., 1988	88 km ± 18 km	−115.60912	36.06631
Las Vegas shear zone	Undetermined	47 ± 7 km	15–11 Ma	11.75 km/m.y.		Alignment of Gass Peak thrust (Sheep Range) with Wheeler Pass thrust (Spring Mt.).	Snow and Wernicke, 2000; Burchfiel et al., 1987; Wernicke et al., 1988			
Sheep Range, Pintwater Range, Spotted Range detachment (26) [59, 61, 64]	23 km	20 ± 5 km	13 Ma–? (9 Ma)	3.67 km/m.y.	N 63 W	Extension associated with the Sheep Range detachment, extension amount based on cross section restoration	Guth, 1989; Snow and Wernicke, 2000; Snow, 1992	74 km ± 11 km	−114.91820	36.63221
Nopah Range, Resting Spring Range, Spring Mtns. detachment (27) [50]	26 km	~25 ± 3 km	14–9 Ma	5 km/m.y.	N 63 W	Alignment of the trace of the Wheeler Pass thrusts with respect to other thrusts in the system	Wermicke et al., 1988, Snow and Wernicke, 2000	113 km ± 18 km	−116.18892	36.27185
Cottonwood, Panamint, Black Mountains/Amargosa, central Death Valley, Emigrant detachments (28, 30, 32) [54]	102 km	104 km ± 7	11–2 (?) Ma	11.5 km/m.y.	N 67 W	The original extent of Eagle Mountain Formation must have been within 20 km of source area in southern Cottonwoods.	Neimi et al., 2001	217 km ± 19 km	−117.15952	36.20316
Resting Springs, Nopah Ranges and Black, Panamint Mountains/ Grapevine, Amargosa, central Death Valley area detachments (27, 28, 30)	105 km	100 ± 7	9–5 Ma	22.5 km/m.y.	N 78 W	Willow Spring pluton intruded (10-12 km) at 11.6 cooled rapidly (6-7 Ma) and appears in boulders at ~5 Ma. (Amargosa chaos). Alignment of thrust-belt structures	Wernicke et al., 1988; Snow and Wernicke, 2000; Holm et al., 1992; Holm and Dokka, 1993; Snow, 1992			
Kingston Range/Kingston Range detachment (29) [38]	6 km	6 km	13.1–12 Ma	6 km/m.y.	E-W	Deposition in the Shadow Valley Basin	Fowler and Calzia, 1999		−115.88365	35.68015
Southern Black Mountains/ Kingston Range, Amargosa detachments (30) [52]	25 km	25 ± 3 km	12–8 Ma	6.25 km/m.y.	E-W	Granite megabreccias (in the greater Amargosa basin) possibly derived from a displaced portion of Kingston Range pluton (west of basin).	Snow and Wernicke, 2000		−116.59671	36.03965
Funeral, Grapevine Mountains/ Point of Rocks detachment (31) [60]	Undetermined	~10 km	14–10 Ma	2.5 km/m.y.	N 45 E	Opening of the extensional Bullfrog Basin	Cemen et al., 1985; Snow and Lux, 1999		−116.87030	36.68789
Grapevine Mountains, Bare Mountain/Bullfrog detachments (31) [72, 58]	60 km	52 ± 2	14–7 Ma	7.43 km/m.y.	S 68 E	Cordillera fold-thrust belt reconstructions	Snow and Wernicke, 2000, 1989		−116.67924	36.87579
Grapevine Mountains, Funeral Mountains/Boundary Canyon detachment (31) [72]	32 km	35 ± 2 km	9–5 Ma	8.75 km/m.y.	S 37 E	Cordillera fold-thrust belt reconstructions, AFT, ZFT and sphene FT cooling ages	Snow and Wernicke, 2000, 1989; Snow, 1992, Hoisch and Simpson, 1993; Holm and Dokka, 1991		−117.21776	37.12056
Northern Death Valley		20 ± 10	5–0 Ma	2-6 km/m.y.	E-W	Offset thrust fault and Quaternary markers	Reheis 1993, Reheis and Sawyer, 1997			
Cottonwood Mountains/ Emigrant fault system (32) [70]	22 km	22 ± 3 km	6–3.2 Ma	5.5 km/m.y.	S 45 E	Correlation of White Top backfold in Cottonwood, Funeral Mountains and Specter Range	Wernicke et al., 1988; Snow, 1992; Snow and Lux, 1999; Snow and Wernicke, 2000		−117.57841	36.87160
Darwin Plateau, Inyo Mountains/Hunter fault (33) [51, 66]	9 km	9 ± 1	4.8–0.6 Ma	2.25 km/m.y.	S 55 E	Correlation of Saline Range volcanics	Burchfiel et al., 1987	226 km ± 19 km	−117.66132	36.17492
Sierra Nevada/Owens Valley fault system (34) [65]	~9 km	9 ± 6	0–4 Ma	2.25 km/m.y.	S 60 E	Estimate of 15% ± 10% extension	Wernicke et al., 1988	235 km ± 20 km	−119.80163	37.88503
Total extension	232 km		235 ± 20 km		N 78° W					

Note: Long.—longitude; Lat.—latitude; AFT—Apatite Fission Track cooling age; ZFT—Zircon fission track age; FT—Fission Track. Numbers in parentheses refer to specific ranges identified on Fig. 2; numbers in brackets refer to the RANGE_ID number for individual ranges in the ArcGIS shape files and the Movement Table (ArcGIS files, Movement Table [see footnote 1]). The cumulative error reported in column 9 equals the square root of the sum of the squares for individual vectors.

TABLE 3. DATA USED FOR RESTORING EXTENSION IN SOUTHERN BASIN AND RANGE

Range/fault	Horizontal displacement of range block (model polygon)	Horizontal component of fault Slip (data)	Timing of slip	Rate of deformation (horizontal component of fault slip/duration)	Direction of motion	Data used	References	Long. (x)	Lat. (y)
McCullough Range to Colorado Plateau (35) [37]	80 km	50-80 km	14–16 Ma (24)	8 km/m.y.	S 75 W	Restoration of strike slip fault offsets, tilted volcanic rocks, porphyry copper emplacement depths	Spencer and Reynolds, 1989; John and Foster, 1993	−115.34595	35.17415
Black Mountains (36) [46]	36 km (total)	>25 km	15–13.4 Ma	2.5 km/m.y.	N 70 E	Tilted volcanic rocks.	Foster et al., 1993; Spencer et al., 1995; Spencer and Reynolds, 1989	−114.49030	35.47688
Sacramento, Chemehuevi Eldorado Mountains (37) [44]	36 km	>25–30 km	21–15 Ma	5 km/m.y.	S 60 W	Ar/Ar, AFT cooling ages	John and Foster, 1993	−114.76854	35.31117
Buckskin, Rawhide Mountains (38) [629]	66 km	66 km ± 8 km	27–13 Ma	4.7 km/m.y.	S 57 W	Timing indicated by tilted volcanic strata, magnitude determined by offset necessary to expose lower plate	Scott et al., 1998; Foster et al., 1993; Spencer et al., 1995; Spencer and Reynolds, 1991	−113.74331	34.09275
Catalina, Rincon Mountains (39) [648]	28 km	20–30 km, could be up to 40 km	27–20 Ma	4 km/m.y.	S 60 W	Correlation of Precambrian granite and pre-mid Tertiary thrusting	Davy et al. 1989; Dickinson, 1991; Fayon et al., 2000	−110.71584	32.35001
Harquahala, Harcuvar Mountains (40) [657]	66 km	67 km ± 17 km	26–14 Ma	5.6 km/m.y.	S 57 W	Displaced breccias (55 km) plus additional extension in volcanic and Precambrian rocks (12 ± 7)	Richard et al., 1990; Spencer and Reynolds, 1991.	−113.51995	33.86443
Pinaleno Mountains (41) [647]	22 km	20–30? km	29–19 Ma	2.5 km/m.y.	S 60 W	Ar/Ar cooling ages, approximate amount of displacement necessary to expose lower plate	Long et al., 1995	−110.01163	32.77288
South Mountain (43) [653,654]	50 km		25-19 Ma		S 60 W		Reynolds, 1985	−111.60311	33.13175
Whipple Mountain (44) [665]	63 km	71 km ± 19 km	22–16 Ma	11.8 km/m.y.	S 57 W	Offset of dike swarm, tilted sedimentary strata	Davis and Lister, 1988; Spencer and Reynolds, 1991	−114.10627	34.31624
Rio Grand extension (45)	7 km	6 km	12–18 Ma	.875 km/m.y.	38°N	palinspastic restoration of seismic controlled cross section, and growth strata in basin	Chapin and Cather, 1994; Ingersoll, 2001; Russell and Snelson, 1994		
	13 km	10 km	12–18 Ma	1.625 km/m.y.	36°N		Chapin and Cather, 1994; Ingersoll, 2001; Russell and Snelson, 1994		
	17 km	17 km	12–18 Ma	2 km/m.y.	35°N		Chapin and Cather, 1994; Ingersoll, 2001; Russell and Snelson, 1994		

Note: Long.—longitude; Lat.—latitude; AFT—Apatite Fission Track cooling age. Numbers in parentheses refer to specific ranges identified on Fig. 2; numbers in brackets refer to the RANGE_ID number for individual ranges in the ArcGIS shape files and the Movement Table (ArcGIS files, Movement Table [see footnote 1]).

Malin, 1992; Walker et al., 1995; Glazner et al., 2002).

Following this early phase of extensional deformation, a system of right- and left-lateral strike-slip faults similar to those active today was established, with right-lateral shear along a series of northwest-striking faults predominant (Fig. 5). The total accumulated shear across the Mojave, as documented by field studies, is 53 km ± 6 km (Table 4). The timing of right-lateral shear is not well constrained. Motion on the faults is inferred to be post–10 Ma based on strain compatibility with deformation directly north and south (Tables 2 and 5).

Vertical Axis Rotations East of the San Andreas Fault

There are two zones of vertical-axis rotation east of the San Andreas fault: the Eastern Transverse Ranges located immediately south of the Mojave block and the northeastern Mojave rotational block (Carter et al., 1987; Schermer et al., 1996; Dickinson, 1996) (Fig. 5 and Table 4).

The Eastern Transverse Ranges include a series of structural panels separated by east-west–oriented, left-lateral faults (Dickinson, 1996). Paleomagnetic studies show that 10 ± 2 Ma rocks within this zone record the entire 45° rotation (Carter et al., 1987), while 4.5 Ma volcanic rocks are unrotated (Richard, 1993). These constraints imply that all of the rotation and most of the right-lateral strike-slip motion in the Mojave region immediately to the north are ca. 10 Ma and younger.

The northeastern corner of the Mojave region is another area of pronounced clockwise rotation. Schermer et al. (1996) proposed that the northeastern Mojave underwent 23° of rotation accompanied by 5 km of left-lateral slip on faults within the rotating region and 15° of ''rigid body'' rotation. Total right-lateral shear predicted by this model is 33 km.

San Andreas System and Areas to the West

Deformation west of the San Andreas fault is defined by four first-order constraints (Fig. 6 and Table 6). The first is motion on the San Andreas fault itself, which is tightly constrained in central California at 315 km ± 10 km by restoring the Pinnacles volcanics west of the fault to the Neenach volcanics to the east of it (Matthews, 1976; Graham et al., 1989; Dickinson, 1996). The offset volcanics were extruded from 22 Ma to 24 Ma, but tentatively correlative late Miocene strata (7–8

TABLE 4. DATA USED FOR RESTORING STRIKE-SLIP DISPLACEMENTS IN THE MOJAVE REGION

Fault	Horizontal displacement of range block (model polygon)	Horizontal component of fault slip (data)	Timing of slip	Data used (offset features)	References	Cumulative displacement of right-lateral fault slip data (± cumulative error)
Central Mojave (41)	63 km	40–50 km	24-18 Ma	Offset features that include Jurassic dikes, intrusive rocks, and shelf to ocean facies transition	Glazner et al., 1989; Martin et al., 1993; Fletcher et al., 1995; Ingersoll et al., 1996	
Aztec Mines Wash fault	8 km	8 km LL	post lower Miocene	Intrusive contact between San Gabriel terrane and Cretaceous pluton	Powell, 1981	
Blue Cut fault	4 km	6-9–9 km		Antiform in gneissic foliation	Hope, 1966	
Bullion/Rodman/Pisgah fault	13 km	6.4–14.4 km RL		Kane springs fault	Dokka, 1983	10.4 km ± 4 km
Chiriasco fault	7–16 km	11 km LL		Dacite dike, and steeply dipping Red Cloud thrust fault	Powell, 1981	
Chuckwalla Valley basin	31 km (RL)	gravity low		Gravity data indicate complex basin structure	Rotstein et al., 1976; Richard, 1993	
Cibola fault	7 km	7 km RL		West dipping normal faults, and east dipping contact between lavas	Richard et al., 1992	
Ford Lake North basin	5 km	3.5 km RL		Base of McCoy Mountains formation	Stone and Pelka, 1989	
Indian Wash Basin	7 km	7 km RL		Stratigraphic separation	Richard, 1993	
Iron Mountains fault	5 km	5.5 km RL		Rock units (unspecified)	Howard and Miller, 1992	
Laguna fault system	36 km	2 km RL		Slip estimated by estimating extension necessary for 20° dip in conglomerate	Richard, 1993	
Mammoth Wash fault	~12 km	~9 km LL		Intersection of greenschist with Chocolate Mountain Thrust	Dillon, 1975	
Maria fault		4.5 km RL		Thrust faults and syncline	Hamilton, 1987; Ballard, 1990	
Mesquite Lake fault		3.5 km RL		Folds in Pleistocene sediments	Bassett and Kupfer, 1964	
Packard Well fault	16 km	16 km RL		Mesozoic rocks and structures	Powell, 1981; Richard and Dokka, 1992	
Pinto Mountain fault	not available	18–22 km LL		Intrusive contacts	Hope, 1966; Dibblee, 1982	
Salton Creek fault	8 km	8 km LL		Correlation with Aztec mines fault	Powell, 1981	
Sheep Hole, Dry Lakes fault	31 km	23 km RL/11 km RL	to early Pleistocene	Photo interpretation	Powell, 1981; Howard and Miller, 1992	
Valley Mountain fault	21 km	6.5–14.4 km RL			Dokka, 1983; Richard, 1993	
Cleghorn Pass fault	valley mt offset	12 km RL	to early Pleistocene	Intrusive contacts	Howard and Miller, 1992	
Cleghorn Lakes fault	''	3 km RL	to early Pleistocene	Intrusive contacts	Howard and Miller, 1992	
Cadiz Lake fault	16–25 km	25 km RL	to early Pleistocene	Roof pendants with distinctive lithology	Howard and Miller, 1992	
Broadwell Lake fault	6 km	6 km RL	to early Pleistocene	Miocene strata	Howard and Miller, 1992	16 km ± 4 km
South Bristol fault	9 km	6.5 km RL	to late Pleistocene	Mesozoic granitites, metavolcanics	Howard and Miller, 1992	22.5 km ± 4 km
Bristol, Granite Mountain fault	27 km	10 km RL (0-10)		Unknown, or plutons and volcanic rocks	Howard and Miller, 1992; Dokka and Travis, 1990	27.5 km ± 6.4 km
Ludlow	14 km	>6 km RL	to early Pleistocene	Source area for Pleistocene conglomerate	Howard and Miller, 1992	33.5 km ± 6.4 km
Calico	10 km	9.6 km RL		Offset early Miocene fault	Dokka, 1989; Glazner et al., 2002	43.1 km ± 6.4 km
Blackwater	4.5 km	1.8 km	last 3.77 m.y.	Offset volcanics, basement lithologies	Oskin et al., 2004	
Gravel Hills + Harper Lake	12.5 km	3.2 km RL + 3 km RL		Offset lithologies	Dokka and Travis, 1990; Dibblee, 1968	
Camp rock	11 km	4 km RL		Offset basement lithologies	Dokka, 1983; Dibblee, 1964	47.1 km ± 6.4 km
Hendale	4 km	3 km RL		Offset lithologies	Miller and Morton, 1980	50.1 km ± 6.4 km
Lockheart	4 km	>0 RL			Dokka and Travis, 1990	
Lenwood	5 km	2 km RL		Offset volcanics, graben width	M. Strane, Pers. Comm, 2005	53 km ± 6.4 km
NE Mojave rotation	23 km	22–23 km RL		Paleomagnetic rotations	Schermer, 1996; Miller and Yount, 2002	
Total shear in the Mojave	99 km	53 ± 6.4 km				

Note: RL and LL indicate right-lateral motion and left-lateral motion, respectively.

TABLE 5. DATA USED FOR RESTORING VERTICAL AXIS ROTATION IN RECONSTRUCTION

Rotations	Rotation in model	Measured rotations from data	Age	Rate	Direction	References	Long. (x)	Lat. (y)
Colorado Plateau (45) [74]	1.5°	1°–1.5°	12–18 Ma	.1875°/m.y. cw	Paleomagnetism, extension determined through cross section restoration	Chapin and Cather, 1994	−110.14435	37.26894
Eastern Transverse Ranges (46) [90–99]	45°	41.4° ± 7.7	after 10.4 Ma	cw	Paleomagnetic data	Carter et al., 1987		
Northeastern Mojave (47) [mojave 6]	36°–38°	23° locally 63°	after 10.4 Ma	cw	Paleomagnetic data	Schermer et al., 1996		
Jurassic dikes in NE Mojave (47)		40–50°		cw		Ron and Nur, 1996		
Mojave rotations (47)		30°	21–48 Ma	cw	Paleomagnetic data	Dokka and Travis, 1990; Dokka et al., 1998		
Cottonwood and Funeral Mtns. (31, 32) [70, 60]		40°	mid Miocene or later	cw	Paleomagnetic data	Snow and Lux, 1999; Snow and Wernicke, 2000	−117.57841	36.87160
Black Mountains (30) [52]		50–80°	after mid Miocene pluton		Paleomagnetic data	Holm et al., 1993	−116.59671	36.03965
Grapevine Mountains (31) [72]		~20°		ccw	Paleomagnetic data	Niemi, 2002; Snow and Wernicke, 2000	−117.21776	37.12056
Bare Mountain (31) [58]	80°	80°	pre mid-Miocene	cw	Paleomagnetic data	Snow and Prave, 1994	−116.67924	36.87579
Pintwater, Spotted and Specter Range and Stripped Hills (26) [56]		Oroclinal flexure (75–90°)	between 16 and 14 Ma	cw		Carr et al., 1986; Hudson et al., 1994; Niemi, 2002	−116.18407	36.62382
Northern Walker Lane (18–19) [326, 355]		35°–51°	9–13 Ma	cw	Paleomagnetic data on volcanic rocks	Cashman and Fontaine, 2000		
Sierra Nevada (34) [65]	2° (ccw)	6° ± 8°	post Cretaceous	cw	Paleomagnetic data	Frei et al., 1984; Frei, 1986; Bogen and Schweickert, 1985; Gilder and McNulty, 1999	−119.80163	37.88503
Western Transverse Ranges (50)	117°	90°–110°	~15 Ma	6°/m.y. cw	Paleomagnetic data	Hornafius et al., 1986; Luyendyk, 1991		

Note: Table 5 is an incomplete listing of an extensive paleomagnetic data set for western North America. Long.—longitude; Lat.—latitude; cw—clockwise rotations; ccw—counterclockwise rotations. Numbers in parentheses refer to specific ranges identified on Fig 2; numbers in brackets refer to the RANGE_ID number for individual ranges in the ArcGIS shape files and the Movement Table (ArcGIS files, Movement Table [see footnote 1]).

Ma) are apparently offset 255 km (Graham et al., 1989; Dickinson, 1996).

The second constraint is the ~110° clockwise rotation of major fault-bounded blocks in the western Transverse Ranges (Hornafius et al., 1986; Luyendyk, 1991). Because of the length and structural integrity of these blocks (in particular, the Santa Ynez Mountains), this rotation requires a coast-parallel displacement of ~270 km (Hornafius et al., 1986).

The shear and rotation of these blocks are confirmed by the third major constraint, reconstruction of now-scattered outcrops of the distinctive Eocene Poway Group. Exposures along the Channel Islands were rifted away from counterparts in southernmost California, which are in turn offset from their source area in northern Sonora, Mexico, by the southern San Andreas fault system (Abbott and Smith, 1989). Rifting and rotation of the western Transverse Ranges away from the Peninsular Ranges formed the strongly attenuated crust of the Continental Borderlands on their trailing edge. The magnitude of this extension is proposed to be ~250 km based on seismic reflection data delineating the geometry of extensional fault systems and correlation of ''mega key beds'' or lithotectonic belts (forearc basin sediment, Franciscan subduction complex) (Crouch and Suppe, 1993; Bohannon and Geist, 1998).

The final first-order constraint is the opening of the Gulf of California. Although offset of the Poway Group suggests roughly 250 km of displacement, recognition of correlative pyroclastic flows on Isla Tiburon and near Puertecitos on the Baja Peninsula dated at 12.6 Ma and 6.3 Ma constrains the full transfer of Baja California to the Pacific plate to have occurred no earlier than ca. 6 Ma, with 255 km ± 10 km of displacement along the plate boundary since then (Oskin et al., 2001). Including additional deformation of the adjacent continental margins increases the magnitude of displacement to as much as 276 km ± 10 km (Oskin and Stock, 2003).

WESTERN NORTH AMERICA ANIMATION

The western North America animation (Animation 1) combines 13 individual paleogeographic maps (Figs. 7–9) (Appendix 1, paleogeographic maps [see footnote 1])[2] generated by ArcGIS into a digital animation illustrating a model of how extension and right lateral shear evolved in the region. The color scheme

[2]If you are reading this offline, please visit www.gsajournals.org to view Animation 1.

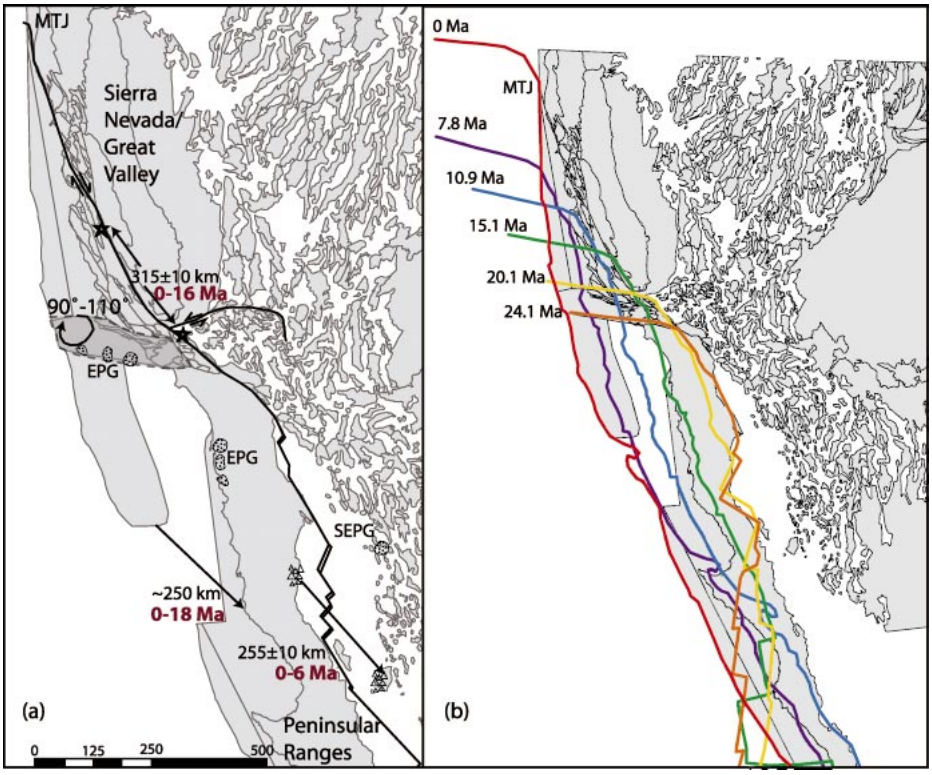

Figure 6. A: First-order constraints for displacement along the San Andreas fault and associated displacements to the west. Arrows indicate approximate magnitude and direction of individual relative displacements between polygons. Black numbers indicate horizontal displacement amount, bold red numbers indicate age range of displacement. Stippled areas labeled EPG show distribution of Eocene Poway Group and equivalents. Stippled area labeled SEPG marks the location of the source area for the Eocene Poway Group. Triangle pattern (Gulf of California), and stars (central California) show distribution of correlative volcanic units offset by the San Andreas–Gulf of California rift system. MTJ is modern location of the Mendocino triple junction. Data from Abbott and Smith, 1989; Bohannon and Geist, 1998; Crouch and Suppe, 1993; Dickinson and Wernicke, 1997; Dickinson, 1996; Graham et al., 1989; Hornafius et al., 1986; Luyendyk, 1991; Matthews, 1979; Oskin et al., 2001. B: Successive locations of the eastern edge of Pacific plate oceanic lithosphere relative to stable North America. The thick colored lines represent minimum extent of oceanic lithosphere at the times shown (from Atwater and Stock, 1998). These positions constrain the maximum westward extent of continental North America through time.

for the animation includes yellow, orange, and red polygons on a white background. The polygon shape reflects the modern bedrock-alluvium contact, fault-bounded crustal blocks or the physiographic boundaries of large, intact crustal blocks. Yellow polygons indicate areas where there are no data for how the region is deforming. Orange polygons (ranges) are ranges whose motion is directly constrained by kinematic data. These polygons turn red during the time period of motion (i.e., Baja California turns red from 6 to 0 Ma as it separates from North America and moves northward on the Pacific Plate). A notable exception to this is the Colorado Plateau–Rio Grand rift area. Neither the Colorado Plateau, nor the Rio Grande rift turn red during rotation and extension even though there are data that describe this deformation (Table 5). The space created (additional white space between the colored polygons) as the movie progresses in time indicate areas of extension. The removal of white space (as polygons move closer together) indicates areas of compression. The thick blue line on the left of the animation represents successive locations of the eastern edge of Pacific plate oceanic lithosphere relative to stable North America at the time period annotated on the upper left edge of the line (from Atwater and Stock, 1998). The position of this line constrains the maximum westward extent of continental North America at the time indicated because it shows the minimum east limit of extant oceanic crust. Details of the reconstruction can be seen by moving the slider bar on the animation. To move back and forth over a narrow window of time, just hold the mouse key down over the triangle on the slider bar and move it back and forth over the time window of interest.

DISCUSSION

The exercise of developing a self-consistent, strain-compatible model has raised a number of issues that are difficult to resolve satisfactorily in the reconstruction and require further investigation. The most apparent (among many!) are (1) the need for middle to late Miocene right-lateral shear in the eastern Mojave region to make room for the northerly motion of the Sierra Nevada determined from the central and northern Basin and Range reconstruction paths; (2) the need for large amounts of relatively young extension in northern Mexico both east and west of the Sierra Madre Occidental to reconcile core complex extension in Arizona and the late Miocene–Pliocene opening of the Gulf of California; (3) the apparent rotational history of the Sierra Nevada–Great Valley block; and (4) generally large amounts of Miocene-Pliocene shortening and extension in the Transverse Ranges, Coast Ranges, and Borderlands provinces, which arise from the need to reconcile San Andreas offset with the position of oceanic crust offshore, differences in the age of extension north and south of the Garlock fault, and large clockwise rotation of the Santa Ynez Mountains block (Animation 1).

Eastern Mojave Region

The eastern California shear zone–Walker Lane belt is an ~120-km-wide zone of right-lateral, intraplate shear east of the Sierra Nevada and San Andreas fault. Geodetically this shear zone accommodates up to 25% of the Pacific–North America relative plate motion (Bennett et al., 2003; McClusky et al., 2001; Miller et al., 2001; Sauber et al., 1994). Geologic estimates of displacements vary along the north-south extent of the eastern California shear zone. Proposed net displacement along the eastern California shear zone (oriented ~N20°W) varies from 65 km in the Mojave region (Dokka and Travis, 1990) to 133 km in the central Basin and Range (Snow and Wernicke, 2000; Wernicke et al., 1988). In the northern Walker Lane region, shear estimates

TABLE 6. DATA USED FOR RESTORING HORIZONTAL DISPLACEMENTS WEST OF THE SAN ANDREAS FAULT

Range/fault	Horizontal displacement of range block (model polygon)	Horizontal component of fault slip (data)	Timing of slip	Rate of deformation (horizontal component of fault slip/duration)	Direction of motion	Data used	References
San Andreas motion (48)	310 km: 0–6 Ma, 174 km; 8–12 Ma, 89 km; 14–16 Ma, 47 km	315 km ± 10 km	0–5 Ma, 170 km ± 5; 0–10 Ma, 289 km ± 9; 0–16 Ma, 315 km ± 10	0–5 Ma, 34 km/yr; 0–10 Ma, 24 km/yr; 0–16 Ma, 4.3 km/yr	N 30 W	Offset of Holocene geological features, early Miocene volcanic and sedimentary rocks and Miocene sedimentary breccias	Atwater and Stock, 1998; Dickinson and Wernicke, 1997; Dickenson, 1996; Graham et al., 1989; Sieh and Jahns, 1984; Matthews, 1979
Baja/Isla de Tibron (49) (51) [85] [109]	300 km	276 km ± 13 km	6–0 Ma	43.5 km/yr	N 50 W	Correlating Miocene volcaniclastic strata	Oskin et al., 2001; Oskin and Stock, 2003
Isla de Tibron/Sonora (51) [109] [170] western Transverse Ranges (50)	50 km	20 km ± 10 km	pre-12 Ma		N 50 W	Correlating Miocene volcaniclastic strata	Oskin and Stock, 2003
Eocene Poway Group	Places San Miguel, Santa Rosa, and Santa Cruz Islands just north of San Diego					Correlation of distinctive volcanic clasts with source area in Sonora Mexico	Abbott and Smith, 1989
Borderland extension	305 km at N 67 W	~250 km	~18 Ma	14 km/m.y.	~N 40 W	Seismic reflection data, correlation of "mega keybeds"	Crouch and Suppe, 1993; Bohannon and Geist, 1998

Note: Numbers in parentheses refer to specific ranges identified on Fig. 2, numbers in brackets refer to the RANGE_ID number for individual ranges in the ArcGIS shape files and the Movement Table (ArcGIS files, Movement Table [see footnote 1]).

range from 20 km to 54 km (Faulds et al., 2005; Hardyman et al., 1984), plus an additional component of northwest-directed extension due to a change in extension direction in the northern Basin and Range from east-west in the east to northwest-southeast in the west.

One of the goals of this study was to develop a kinematically consistent model of the eastern California shear zone that fits within the errors provided by both local and regional studies. We found 100 km ± 10 km right-lateral shear oriented N25°W was compatible with data in both the northern and central Basin and Range (Animation 1). In the Mojave region of the eastern California shear zone, however, available data suggest no more than 53 km ± 6 km of right-lateral shear oriented N25°W, about half of what is required to the north. Kinematic compatibility with the magnitude of deformation north of the Garlock fault requires ~100 km of right-lateral shear though the Mojave region, with the majority of additional shear located on the eastern edge of the shear zone during its early (12–6 Ma) history (Figs. 5,7,8, Animation 1). The 27 km and 45 km of right-lateral offset along the Bristol Mountains–Granite Mountain and southern Death Valley fault zones is significantly greater than previous estimates (0–10 km and 20 km, respectively), but solid piercing points that limit the net offset are scarce and debatable (Howard and Miller, 1992; Dokka and Travis, 1990; Davis, 1977). The ~30 km of displacement along the eastern edge of the Mojave must be transferred southward along the Sheep Hole fault to the Laguna Fault system of Richard (1993). The 36 km of model offset is significantly greater than the 2 km of right-lateral offset proposed by Richard (1993) (Table 4, Fig. 5). Additional faults with significantly greater offsets than that documented by geology are the 11–13 km model offsets on the Camp Rock, Gravel Hills, and Harper Lake fault systems, where current estimates suggest no more than 3 km of offset on any of these faults (Dibblee, 1964; Oskin and Iriondo, 2004; M. Strane, 2005, personal commun.). The difference between the model and data requires that the slip discrepancy must be taken up on other faults (most likely to the east) in the Mojave shear system. Although the details concerning both timing and distribution of shear within the eastern California shear zone will continue to evolve with time, the strength of the central Basin and Range offsets combined with kinematic compatibility constraints require reevaluation of geologic evidence for total magnitude of right-lateral shear through the Mojave. Therefore, we have modeled many of the faults in the

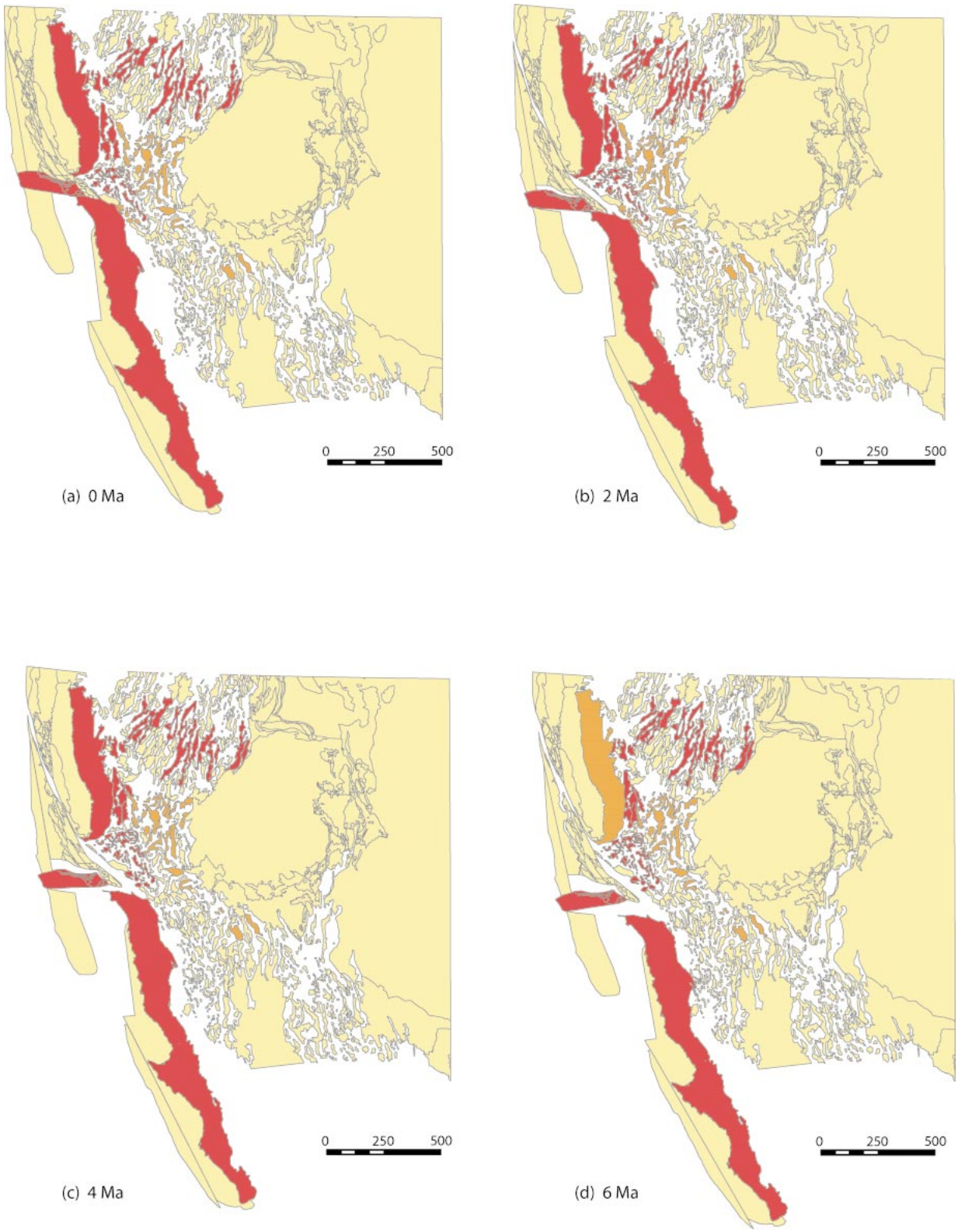

Figure 7. Reconstructed paleogeographic maps (from 0–6 Ma) used in the reconstruction. The color scheme is the same as that for the animation, yellow polygons on a white background. Yellow polygons indicate areas where there are no data for how the region is deforming. Polygons (ranges) that have data associated with their motion are orange when associated faulting is inactive and red during fault activity. Panels represent different time slices: (a) 0 Ma, (b) 2 Ma, (c) 4 Ma, and (d) 6 Ma.

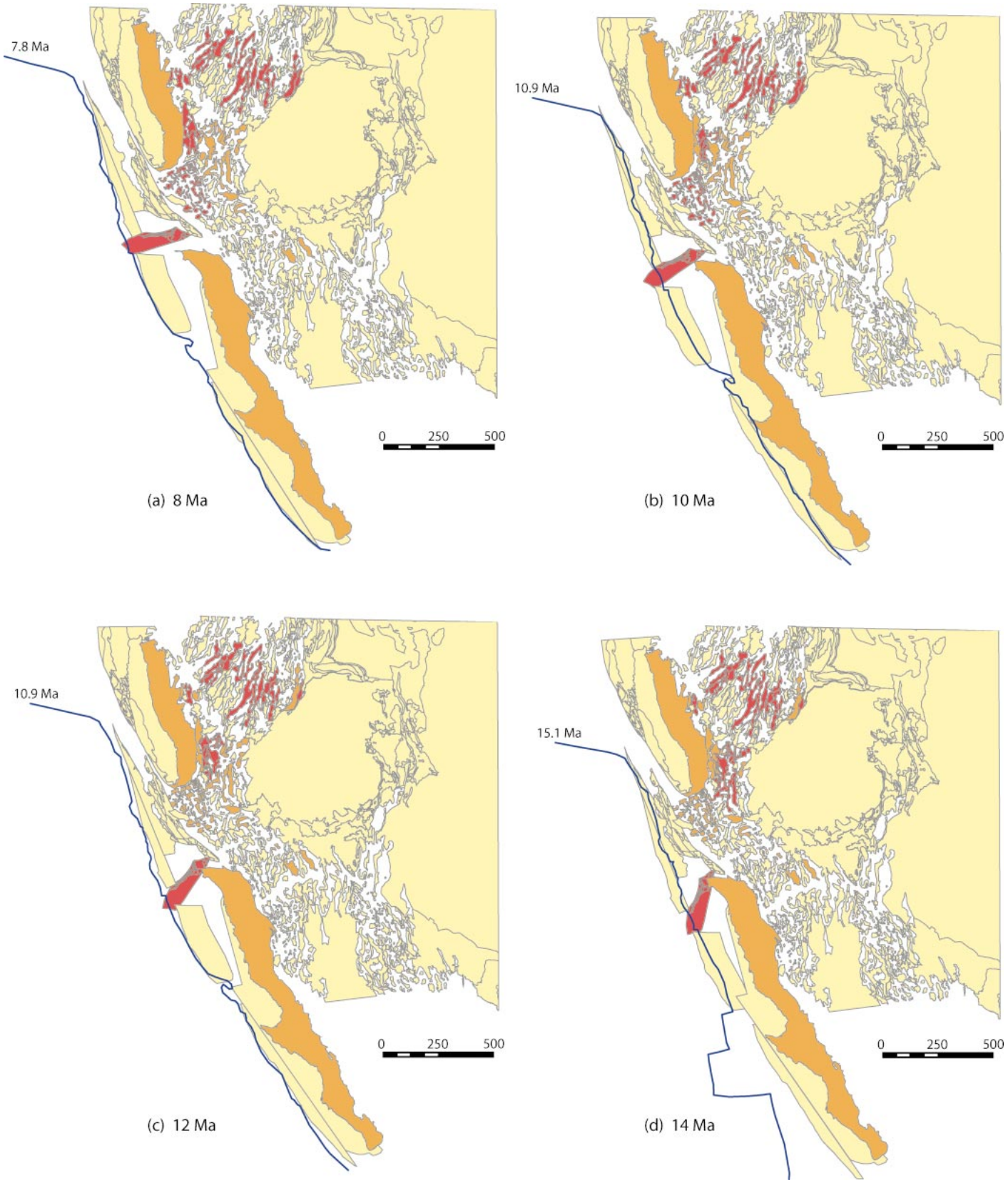

Figure 8. Reconstructed paleogeographic maps (from 8 to 14 Ma) used in the reconstruction. The color scheme is the same as Figure 7. Panels represent different time slices: (a) 8 Ma, (b) 10 Ma, (c) 12 Ma, and (d) 14 Ma.

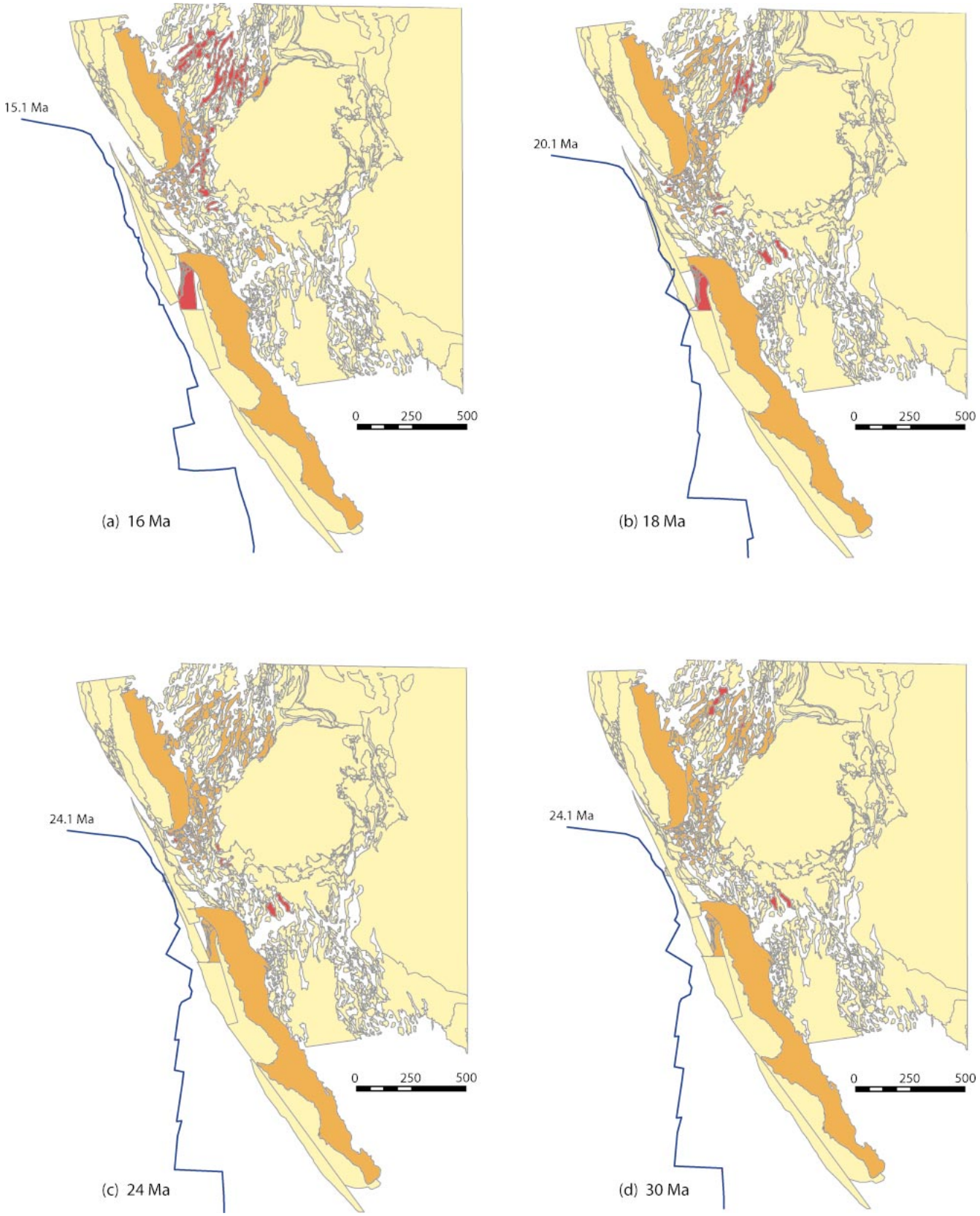

Figure 9. Reconstructed paleogeographic maps (from 16 to 36 Ma) used in the reconstruction. The color scheme is the same as Figure 7. Panels represent different time slices: (a) 16 Ma, (b) 18 Ma, (c) 24 Ma, (d) 30 Ma, and (e) 36 Ma.

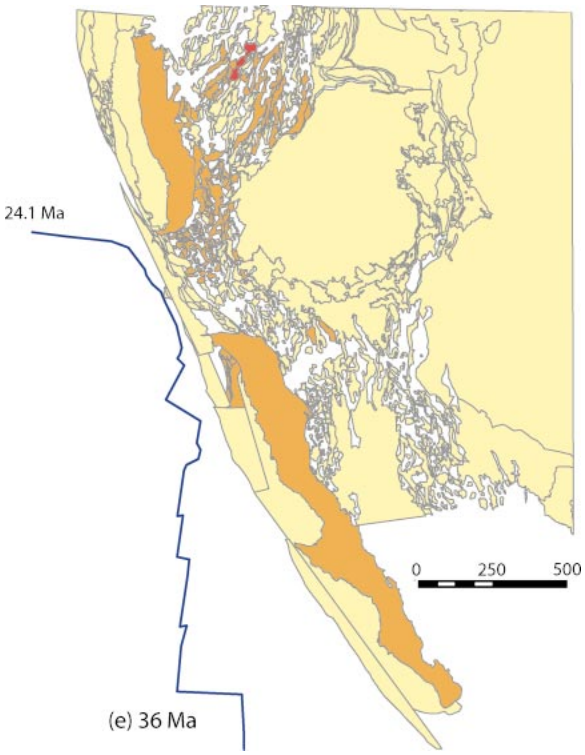

Figure 9. (*continued*).

Mojave with greater net offset than suggested by offset markers. From the model slip amounts shown on Figure 5, we obtain 100 km of right-lateral shear oriented N25°W since 12 Ma, at a long-term rate of 8.3 mm/yr ± 1 mm/yr. We suggest that the discrepancy may be due to penetrative shear in the largely granitic crust between the strike-slip faults (e.g., Miller and Yount, 2002).

Increasing right-lateral shear in the eastern Mojave has implications on how shear is distributed along the entire plate boundary. Since much of the additional shear predates the opening of the Gulf of California (Oskin et al., 2001), it implies ~50 km of dextral shear between 6 and 12 Ma in the Sonora region. The total magnitude of separation of the Baja Peninsula from Sonora predicted from the model is 350 km, 300 km of which is post 6 Ma. This is slightly greater than the 296 ± 20 km, 276 ± 10 km of which is post 6 Ma measured by Oskin and Stock (2003), but still significantly less than the 450 km total continental separation proposed by Fletcher (2003).

Dokka and Travis (1990) proposed that the eastern California shear zone accommodated 9%–14% of total predicted relative motion between plates if shear initiated at 10 Ma. The model of eastern California shear zone deformation that we propose here (Animation 1) suggests that eastern California shear zone deformation is ~28% of San Andreas motion averaged since 12 Ma and 15% of total plate motion since 16 Ma.

Arizona–Mexican Basin and Range

The geographic region that has the fewest local kinematic constraints is Sonora–Chihuahua Mexico. However, the kinematics of Baja California, based on plate tectonic reconstructions (Atwater and Stock, 1998), is an especially powerful constraint on intraplate deformation in this region. The constraint arises from the simple fact that oceanic and continental lithosphere cannot occupy the same surface area at the same time (Atwater and Stock, 1998) (Fig. 6B). The plate tectonic constraint suggests ~330 km ± 50 km of extension between 6 Ma and 24 Ma, because after restoring the offset across the Gulf of California (Oskin et al., 2001; Oskin and Stock, 2003), this is the total overlap between continent and ocean. In concert with strong northeast-southwest extension in Arizona, we suggest similar magnitudes of extension (44 km and 86 km) occurred from 16 Ma to 24 Ma and was oriented N50°E–N60°E (making room for the brown and green curves in Fig. 6B). We show another pulse from 12 Ma to 8 Ma oriented N65°W–N78°W, reflecting the growing influence of the Pacific plate's northerly motion on intraplate deformation, as appears to be the case to the north (Animation 1).

Restoring 330 km of extension, however, particularly the northwesterly extension in the window of time from 16 Ma to 8 Ma, opens up a large northeast-trending gap in southern Arizona and northern Sonora. This gap is a result of differences in both magnitude and timing of extension between southern Arizona and northern Sonora and suggests (incorrectly) that there is ~60 km of NW-SE compression between 16 and 8 Ma (Figs. 8–9). Large magnitude core complex extension in southern Arizona initiates at ca. 28 Ma and wanes from 16 Ma to 14 Ma (Table 3). Significant extension in Sonora occurs over a similar time range (Nourse et al., 1994; Gans, 1997). At ca. 12 Ma, however, significant extension is recorded in both the Gulf extensional province west of the Sierra Madre Occidental (e.g., Stock and Hodges, 1989; Henry, 1989; Lee et al., 1996, Gans et al., 2003) and east of the Sierra Madre Occidental (Henry and Aranda-Gomez, 2000), while only minimal magnitudes of east-west extension are recorded in southern Arizona. This problem is similar to that arising from the difference in timing of extension north of the Colorado River extensional corridor between the Mojave Desert and central Basin and Range. Here, the Garlock fault accommodates different amounts of extension, not only from 10 Ma to the present (Davis and Burchfiel, 1973), but potentially throughout the history of extension in the region (24–0 Ma). Although the difference in timing and magnitude of extension between the Mojave region and the southern Arizona Basin and Range versus the Mexican Basin and Range in Sonora and Chihuahua is generally recognized (e.g., Henry and Aranda-Gomez, 2000; Dickinson, 2002), the geometry and genetic relationship of the transfer system that must separate them is problematic.

In the model presented here, the amount of extension in the Mexican Basin and Range is partitioned between the extending regions east (~134 km) and west (~180 km) of the unstrained Sierra Madre Occidental block. Although both regions display numerous extensional structures, the exact magnitude of extension is unknown. Because of the difference in post–16 Ma extension in Chihuahua and the Rio Grande rift (90 and 20 km, respectively) after ca. 16 Ma, the model includes a zone of right-lateral shear that extends through southeastern Arizona between the two provinces (Animation 1). The existence of this shear zone is unlikely, leaving two possible solutions. The first is that extension systematically increases from the Rio Grande rift to

Chihuahua Mexico due to clockwise rotation of the Sierra Madre Occidental (rotation would need to be greater than the 1.5° rotational opening of the Rio Grande rift). Another solution would be partitioning a much greater magnitude of extension in the Gulf extensional province (~270–300 km), but this is thus far not supported by mapping in the region (Henry and Aranda-Gomez, 2000). Most likely some combination of these factors is necessary to match the first-order geologic constraints of the region.

Sierra Nevada–Great Valley Block Rotation

The reconstruction presented here shows significant extension in the northern Basin and Range between 36 Ma and 24 Ma, with essentially no extension occurring over this time period in the central Basin and Range. To accommodate this difference, the Sierra Nevada–Great Valley Block must rotate or deform internally. We propose that the block behaves fairly rigidly and rotates counterclockwise (Animation 1). After initiation of extension in the central Basin and Range at ~16 Ma, the Sierra Nevada–Great Valley Block rotates clockwise for a final net rotation of 2° (Table 5, Appendix 1, Movement Table [see footnote 1]). The animation shows the early 36–24 Ma rotation accommodated by ~35 km of dextral shear along the proto–Garlock fault and accompanying compression in the southeastern Sierra Nevada region (Animation 1). The actual effects of this rigid body rotation on the deformation of surrounding regions (particularly to the north and south) are highly dependent on the axis of rotation and how rigidly the block behaved, both of which are unknown. The rotation of the Tehachapi Mountains may include this early counterclockwise rotation of the Sierras, as well as potentially being linked to southern Basin and Range core-complex formation, which immediately followed (McWilliams and Li, 1985; Plescia and Calderone, 1986; Walker et al., 1995; Glazner et al., 2002).

Areas West of the San Andreas Fault

Based on the timing and magnitude of displacement on a few fault systems (San Andreas, northern Gulf of California, Mojave, central Basin and Range, and the Santa Ynez Mountains), continental basins must open (creation of white spaces in the movie [Animation 1, Figs. 7–9] suggesting pulses of extension) and close (closing of spaces or overlap of polygons suggesting pulses of contraction) from 24 Ma to 0 Ma. Even at this large and relatively simplified scale, extension and contraction are spatially and temporally complex throughout the region west of the San Andreas fault, and we expect even greater complexities in timing and magnitude at a more detailed level. The following discussion highlights the magnitudes of displacement and summarizes data that either support or conflict with the model displacements.

Transverse Ranges

The clockwise rotation of the Western Transverse Ranges (Hornafius et al., 1986; Luyendyk, 1991) suggests regions of extension and subsequent compression both north and south of the rotating Santa Ynez Mountains block (Fig. 2, range 50) (Animation 1). The magnitude of predicted extension (Fig. 8) and contraction (Fig. 7) (oriented ~north-south) is as great as 130 km to the north of the western side of the block from ca. 12 Ma to the present. Motion of Baja California northward from 6 Ma to the present suggests as much as 90 km of shortening in the southern Transverse Ranges (Santa Ynez and San Gabriel Mountains blocks) (Fig. 7, Animation 1). Transpressive motion involving the San Gabriel Mountains, San Bernardino Mountains, and Mojave blocks implies ~40 km of north-south shortening immediately north of the Peninsular Ranges block. Balanced cross sections through the San Emigdio, Santa Ynez, and San Gabriel Ranges indicate 53 km of shortening since 3 Ma (Namson and Davis, 1988a). Although the shortening estimate is strongly dependent on the details of how the Santa Ynez and Peninsular Ranges–Baja California blocks move, the reconstruction presented here suggests ~60 km of north-south shortening at the longitude of the eastern Santa Ynez Mountains block since 6 Ma. As suggested by Namson and Davis (1988a), shortening of this magnitude in the upper mantle lithosphere is supported by a large volume of high-velocity material imaged tomographically beneath the region (e.g., Humphreys et al., 1984).

Coast Ranges

Differences in the timing of extension within the Mojave and Basin and Range north and south of the Garlock fault, in conjunction with plate tectonic constraints on the westernmost limit of the North America continental edge (Atwater and Stock, 1998), indicate a period of extension (20–16 Ma) and subsequent compression (14–0 Ma) to the west of the Sierra–Great Valley block (Figs. 7–9, Animation 1). Approximately 80 km of core-complex extension south of the Garlock fault occurred prior to significant extension in the central Basin and Range. In order to maintain a quasilinear ocean-continent boundary, a zone of extension roughly equal in magnitude to the core-complex extension is required north of the Garlock fault and west of the Sierra Nevada–Great Valley block. This becomes most visible in the reconstruction at 16 Ma (Fig. 9A). As extension evolves in the central Basin and Range, this same zone undergoes contraction to maintain the quasilinear plate boundary suggested by the extant distribution of oceanic crust from 16 Ma to the present.

The Neogene tectonic and volcanic history from the Great Valley to the edge of the continent is broadly consistent with the model (data summarized in Tennyson, 1989). Although the model and geologic data are difficult to compare quantitatively because there are no obvious normal faults with measurable offsets, the magnitude of extension (and subsequent compression) is significantly less than that predicted by the model. Development of local nonmarine basins and eroded highs, followed by significant subsidence at ~16–18 Ma and the development of the relatively deep marine Monterey basin strongly suggests an extensional event. Rotation of the Tehachapi Mountains and/or extension in the southern San Joaquin Valley (McWilliams and Li, 1985; Plescia and Calderone, 1986; Tennyson, 1989; Goodman and Malin, 1992) may be indicative of this extension but may represent far less than the ~80 km predicted by the model.

The subsequent compression in the Coast Ranges is more quantifiable and appears to be significantly less than that suggested by the model. Estimates of compression in the Coast Ranges east and west of the San Andreas fault range from 20 km to 48 km (Page et al., 1998; Namson and Davis, 1990, 1988b), with all of the known shortening occurring post–10 Ma, and most of it post–4 Ma (Page et al., 1998; Namson and Davis, 1990). Therefore, the model predicts an additional 32–50 km of shortening prior to 10 Ma, for which there is (thus far) no evidence in the Coast Ranges.

Pausing Animation 1 at 15 Ma highlights the crux of the problem (Fig. 9a). To eliminate the need of early 24–16 Ma extension in the Coast Ranges (and subsequent compression), the continental edge would need to bend eastward north of the Mojave and then continue north along the western edge of the Great Valley (Animation 1). This bend in the continental edge would create an ~80-km-wide, ~300-km-long section of oceanic crust that would have to be subducted south of the

northward migrating triple junction during the period of central Basin and Range extension. The solution to the space problem that the model highlights may rest in a combination of several possibilities which include allowing for a warping of the North America coast line, finding greater magnitudes of deformation in the region of the Coast Ranges, and less extension in the central Basin and Range. However, to truly evaluate the magnitude of each of these options requires more detailed reconstruction of crustal blocks west of the San Andreas fault.

Uncertainties in the Reconstruction

Statistically rigorous uncertainties are notoriously difficult to quantify in geological reconstructions, largely because estimates of geologic offset do not have Gaussian or other standard probability distribution functions. The condition of strain compatibility or ''no overlap'' sets a hard limit on the displacement estimate but does not distinguish higher or lower probability of any given position within those limits. Hence, the variance of any given estimate cannot be rigorously quantified.

In map view, any given displacement estimate will have an irregularly shaped uncertainty region. Under the assumption of a uniform probability distribution within these uncertainty regions, Wernicke et al. (1988) used a Monte Carlo method to estimate the total uncertainty on the sum of displacement vectors for a path across the central Basin and Range. This method repeatedly summed randomly selected vectors from each uncertainty region to generate a probability distribution for the net offset. The contour that excluded the outermost 5% of the model runs was taken as an estimate of two standard deviations of the measurement. The estimate of total Sierran motion thus derived was 247 km ± 56 km, S 75° ± 12°E, and therefore a reasonable estimate of the standard deviation would be 28 km. For this same estimate, the square root of the sum of the squares for individual vectors (in the direction of displacement, using values from Table 1 and Figure 10 in Wernicke et al., 1988) is only 15 km. This is perhaps not surprising because the Monte Carlo approach does not place greater weight on values near the center of the uncertainty polygon than on values at the edges.

Our revised displacement estimate for the central Basin and Range, 235 km ± 20 km (again the error is equal to the square root of the sum of the squares for individual vectors), is similar to that of Wernicke et al. (1988) if one considers the 20 km figure as a crude estimate of the standard deviation (1-sigma). However, given the results from Wernicke et al. (1988), the real error may scale upward by as much as a factor of two, depending on the degree to which our best estimate is more probable than values at the extremes. A simple sum of each uncertainty along a given path from Table 1 and Table 2 gives an error estimate of 47 km and 45 km, respectively. Thus, as a rule of thumb, the uncertainty in position of any given range or set of ranges at any given time is on the order of 20–40 km at one standard deviation.

Because the reconstruction involves temporal information (which is also uncertain), the problem of rigorously estimating errors becomes even more difficult and is clearly beyond the scope of this paper. Even though temporal information adds to the uncertainty of position at any given time, the self-consistency of the reconstruction mitigates these uncertainties to a substantial degree.

EVOLUTION OF THE REGIONAL VELOCITY FIELD

Tracking the restored positions of the ranges from the palinspastic maps, we have created ''instantaneous'' velocity fields based on 2 m.y. averages from 0 Ma to 18 Ma and 6 m.y. averages from 18 to 36 Ma. These paleogeodetic velocity fields depict how deformation has evolved in space and time across the plate boundary deformation zone (Figs. 10A–10G).

Figures 10F and 10G (30–18 Ma) illustrate the collapse of the Basin and Range away from the stable Colorado Plateau through the formation of metamorphic core complexes at a time of active ignimbrite volcanism and Pacific-Farallon convergence. Extension initiated first in the northern Basin and Range and then in the southern Basin and Range. This pulse of large-magnitude extension migrated south and north, respectively, until it converged in the central Basin and Range at ca. 16 Ma. Figure 10E (14–16 Ma) emphasizes the large extensional strains in the central Basin and Range especially with respect to the concurrent faulting to the north and south. The 14–16 Ma time slice also shows the impact of the evolving plate boundary on the North American continent as right-lateral shear is accommodated through the rotation of the Western Transverse Ranges and accompanying shear and extension. The 10–12 Ma time slice (Fig. 10D) illustrates the uniform (systematically increasing) strain in the northern Basin and Range and, in contrast, the westward-migrating extension in the central Basin and Range. Significant extension is also necessary in the Mexican Basin and Range due to plate-boundary constraints. It is during this time period that right-lateral shear migrates farther inboard into the continent through the development of the eastern California shear zone. South of the Garlock fault, the shear is oriented nearly parallel to the plate boundary (N25°W). North of the Garlock fault, the shear plus extension creates a more oblique orientation of shear (~N67°W). From 6 Ma to 8 Ma, this same pattern of intracontinental right-lateral shear strengthens with shear partitioned differently south of the Garlock fault than in the central Basin and Range and northern Basin and Range portions of the eastern California shear zone (Fig. 10C). In the Mexican Basin and Range, deformation wanes and extension and right-lateral shear become concentrated in the proto–Gulf of California.

The differences in the velocity fields from the 2–4 Ma average to the 0–2 Ma average is most likely a function of limitations in the data, rather than a significant slowing in the rate of deformation over the last 2 m.y. (i.e., the Mojave region) (Figs. 10A and 10B). Within the model, the lack of timing constraints for right-lateral faults through the Mojave means that the rate of deformation there becomes a function of the rate of deformation to the north and south. North of the Garlock fault, large magnitudes (104 km) of oblique extension are focused predominately from 11 Ma to 3 Ma (Niemi et al., 2001; Snow and Wernicke, 2000; Snow and Lux, 1999). South of the Mojave, the timing of deformation is partially bracketed by the age of rotation of the Eastern Transverse Ranges (as mentioned earlier, ca. 10 Ma rocks record the entire 45° of rotation whereas ca. 4 Ma rocks indicate no rotation; Carter et al., 1987; Richard, 1993). These timing constraints suggest most of the deformational shear in the Mojave occurred between 10 Ma and 2 Ma. However, the total displacement across the eastern California shear zone (100 km ± 10 km) averaged over the last 12 m.y. suggests a long-term rate of 8.3 mm/yr ± 1 mm/yr. This rate is similar to or slightly less than the 8–12 mm/yr rate suggested by geodetic studies (McClusky et al., 2001; Miller et al., 2001; Sauber et al., 1994; Savage et al., 1990).

Another way to look at the evolution of the velocity field and provide a direct comparison between geologic data and geodynamical model results is by mapping the paths that individual ranges take over the deformational interval of interest (Fig. 11). Note that the bend in the path of the Pacific plate does not appear to be related to changes in the paths of

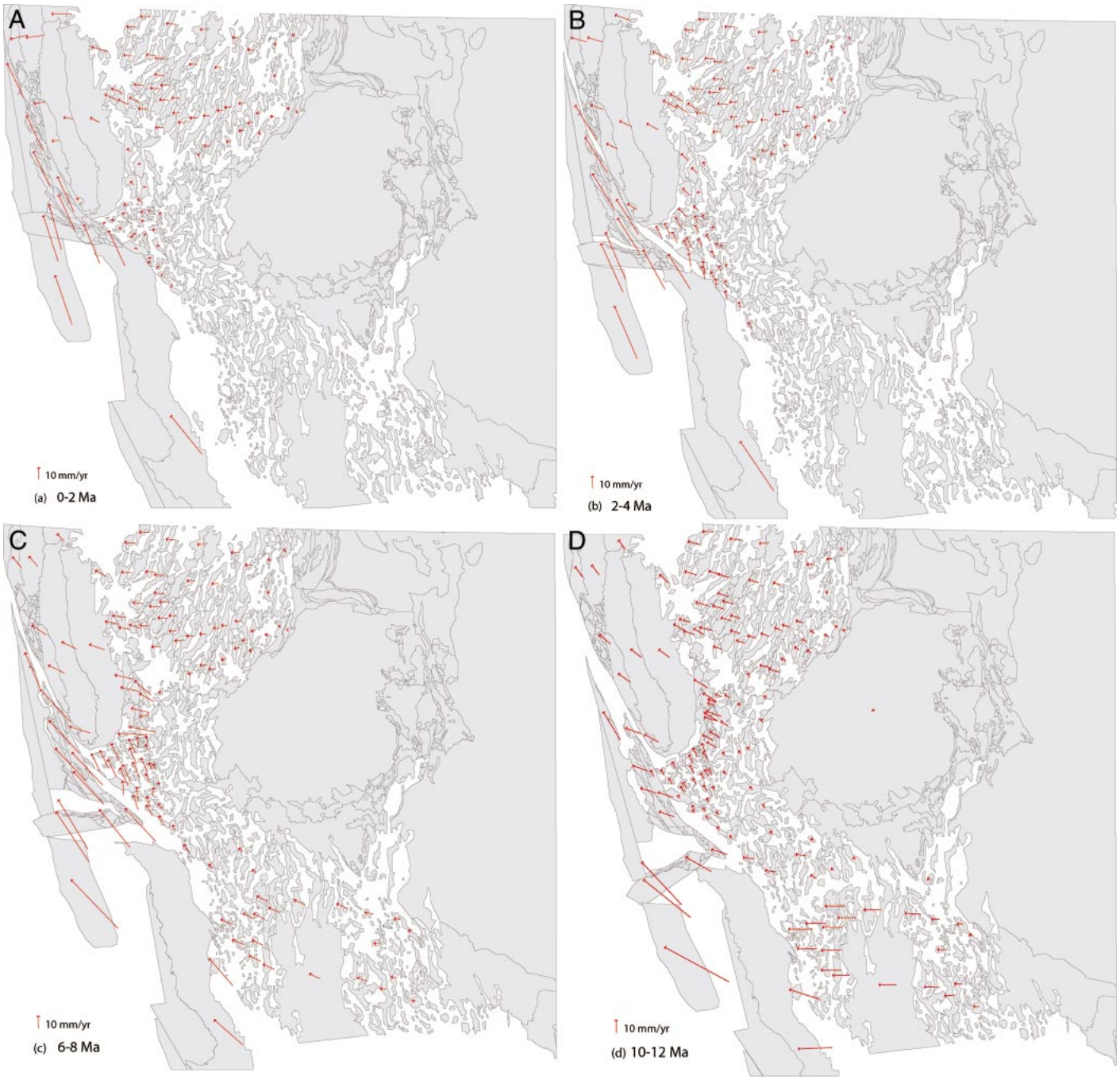

Figure 10. "Instantaneous" velocity fields based on 2 m.y. averages from 0 to 18 Ma, and 6 m.y. averages from 18 to 36 Ma. Arrows show displacement with respect to stable North America and were determined by connecting the centroids of specific ranges at one time with the centroid of the same range in a later time. Because the motion of individual ranges can be very slight at the eastern edge of the model, the line lengths representing each incremental offset were uniformly doubled. Map base is the palinspastic map from the youngest time in the 2 or 6 m.y. interval.

the Sierra Nevada with respect to the Colorado Plateau or changes in the paths of individual ranges within the continent. The most significant continental change in direction occurs at 12 Ma. Because the plate constraints do not require the bend to occur at that time (it is only a function of the times at which magnetic anomalies constrain the position), it is possible within the uncertainties of both the plate reconstruction and geological reconstruction (Atwater and Stock, 1998; Wernicke and Snow, 1998) that these events more closely correlate. As stated previously, the timing of development of right-lateral shear depends on the orientation and timing of early extension in the Death Valley region, which if relatively minor prior to 11 Ma would point toward a later time of onset of right-lateral shear in-

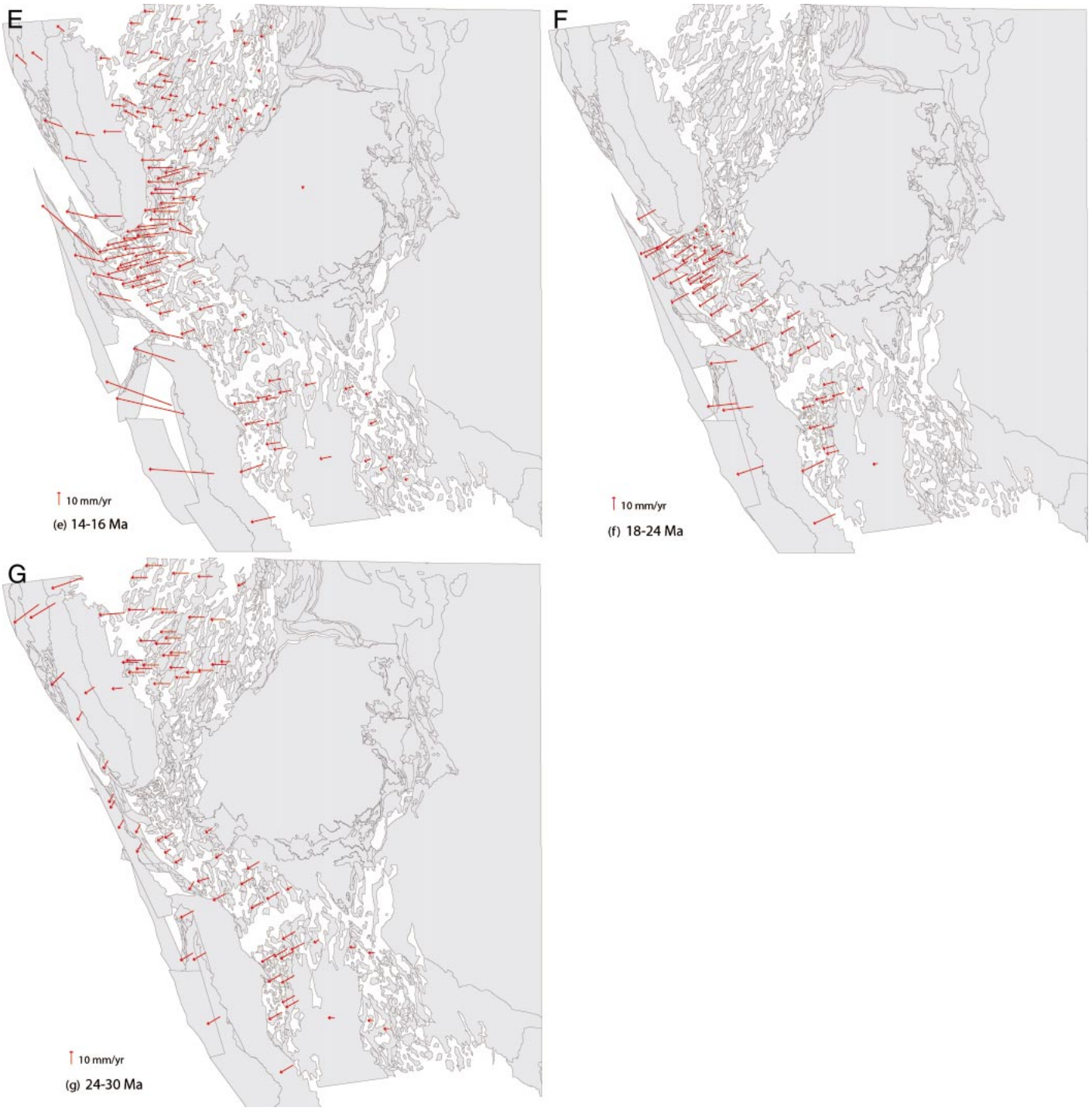

Figure 10. (*continued*).

board of the Sierra Nevada. The distribution of north-northwest shear through the Mojave is kinematically linked to the northwesterly motion of the Sierra Nevada–Great Valley block, in turn requiring at least some amount of right-lateral shear within the Mojave region between 12 Ma and 8 Ma.

CONCLUSIONS

Although orogen-scale reconstructions of the Basin and Range will continue to evolve with time and adjust as more data is acquired, the exercise in kinematic compatibility we present here highlights what we understand and more importantly what we still do not understand regarding the evolution of the plate boundary.

Results that are robust and highlight what we do understand include: (1) 235 km ± 20 km of extension oriented N78°W in both the northern (50% extension) and central (200%

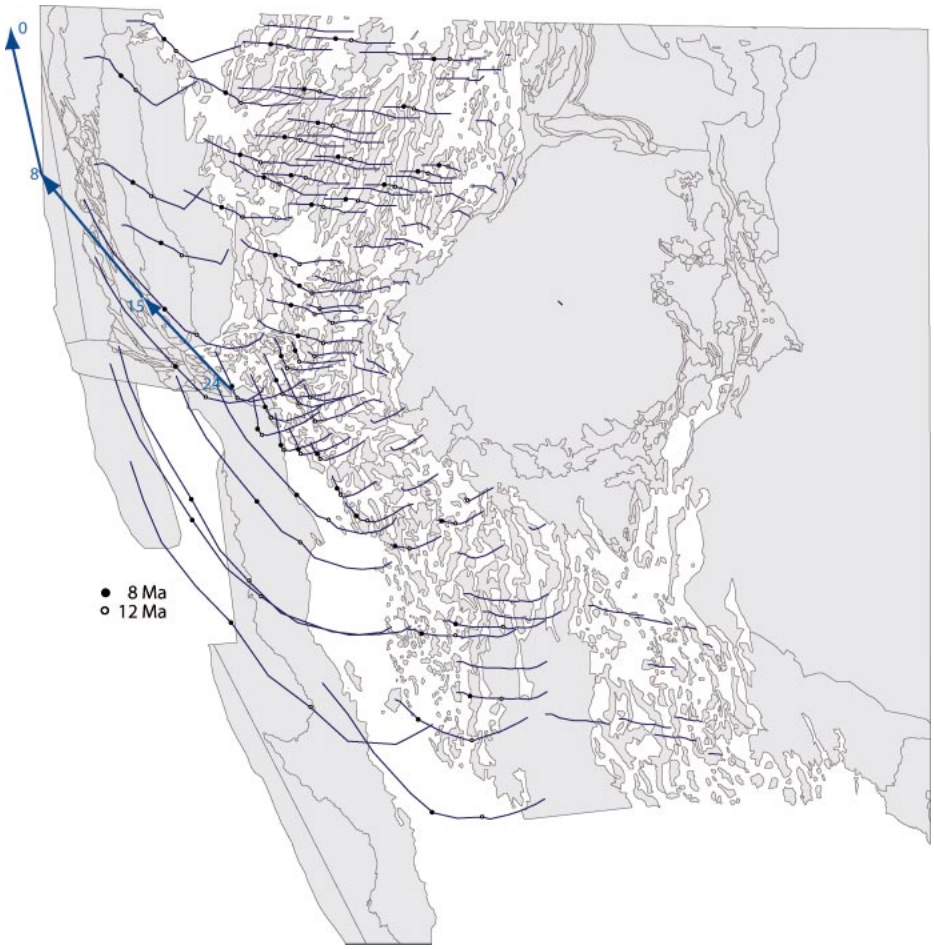

Figure 11. Map illustrating paths of various ranges from 0 to 36 Ma. Solid black circles indicate the positions of the ranges at 8 Ma, and open circles represent the positions of the ranges at 12 Ma. The westernmost point on each line represents the current location of each range. The easternmost point on the path represents the location of the range at 36 Ma. The blue arrows represent the motion of the Mendicino triple junction, with its position shown at 24, 15, 8, and 0 Ma (Atwater and Stock, 1998).

extension) parts of the province. An important implication of the model is that any significant change in extension amount in a portion of the region (i.e., a range on the path between the Colorado Plateau and the Sierra Nevada) must be evaluated in light of how that change affects coevolving regions to the north and south. (2) A significant portion of boundary-parallel shear (in contrast to earlier extension) jumped into the continent at ca. 10–12 Ma, and once established, appears to have migrated westward with time. (3) The magnitude of slip on the eastern California shear zone appears to be 100 km ± 10 km, although the exact structures that accommodate this shear in the Mojave, or how much of the relative motion is accommodated by distributed shear, is not known.

Problems with the current reconstructions are highlighted by large gaps in the model. These zones emphasize areas where more work is needed in refining our ideas about how intraplate deformation is accommodated through time. Salient aspects of the model that we do not understand include: (1) compatibility between timing of extension north and south of the Garlock fault and a smooth north-northwest–trending continental edge as implied by plate tectonic reconstructions. To maintain a relatively smooth continental edge with different periods of extension across the Garlock fault, a triangular window of significant extension (>50 km; 24–16 Ma) followed by an equal amount of shortening (14–0 Ma) would have occurred in the Coast Range–Great Valley region. While known geology supports extension and subsequent compression in these time windows, the magnitude is ~25% of what is needed; and (2) differences in magnitude and timing of extension between southern Arizona and northern Sonora, Mexico, require a transfer zone or large lateral displacement gradient. The model displays this zone as a gap that opens up (going backward with time) between the two provinces. Timing and magnitude of extension in the Sonora region were constrained only by plate motions to the west and broad assumptions as to similarities in timing and direction with areas to the north. Data detailing the magnitude, timing, and direction of extension through the Mexican Basin and Range is necessary to resolve this problem.

ACKNOWLEDGMENTS

This paper has benefited greatly from many conversations with scientists familiar with western North America geology. We specifically want to acknowledge Tanya Atwater, Bill Dickinson, Allen Glazner, Steve Graham, Jon Spencer, Joann Stock, Nathan Niemi, Mike Oskin, Jason Saleeby, and John Suppe. We are grateful to Melissa Brenneman at the University of Redlands for creating the ArcMap document and script used for the reconstruction. The movie would not exist without the help of the University of California, Santa Barbara, Educational Multimedia Visualization Center, specifically Carrie Glavich and Grace Giles. Gary Axen, Doug Walker, Craig Jones, and Randy Keller all provided insightful feedback through the review processes that greatly improved the clarity of presentation. This project was funded by the Caltech Tectonics Observatory.

REFERENCES CITED

Abbott, P.L., and Smith, T.E., 1989, Sonora Mexico, source for the Eocene Poway conglomerate of southern California: Geology, v. 17, p. 329–332, doi: 10.1130/0091-7613(1989)017<0329:SMSFTE>2.3.CO;2.

Allmendinger, R.W., Farmer, H., Hauser, E.C., Sharp, J., Von Tish, D., Oliver, J., and Kaufman, S., 1986, Phanerozoic tectonics of the Basin and Range—Colorado Plateau transition from COCORP data and geologic data, *in* Barazangi, M., and Brown, L.D., eds., Reflection seismology: The continental crust: American Geophysical Union Geodynamics Series, v. 14, p. 257–268.

Allmendinger, R.W., Royse, F., Anders, M.H., Christie-Blick, N., and Wills, S., 1995, Is the Sevier Desert reflection of west-central Utah a normal fault?: Comment: Geology, v. 23, p. 669–670, doi: 10.1130/0091-7613(1995)023<0669:ITSDRO>2.3.CO;2.

Anders, M.H., and Christie-Blick, N., 1994, Is the Sevier Desert reflection of west-central Utah a normal fault?: Geology, v. 22, p. 771–774, doi: 10.1130/0091-7613(1994)022<0771:ITSDRO>2.3.CO;2.

Atwater, T., 1970, Implications of plate tectonics for the Cenozoic tectonic evolution of western North America: Geological Society of America Bulletin, v. 81, p. 3513–3536.

Atwater, T., and Stock, J., 1998, Pacific–North America Plate tectonics of the Neogene southwestern United States; an update, *in* Ernst, W.G., and Nelson, C.A., eds., Integrated Earth and environmental evolution of the southwestern United States: The Clarence A. Hall, Jr. volume: Columbia, Bellwether Publishing, p. 393–420.

Axen, G.J., Wernicke, B.P., Skelly, M.J., and Taylor, W.J., 1990, Mesozoic and Cenozoic tectonics of the Sevier

thrust belt in the Virgin River Valley area, southern Nevada, *in* Wernicke, B., ed., Basin and Range extensional tectonics near the latitude of Las Vegas, Nevada: Boulder, Colorado, Geological Society of America Memoir 176, p. 123–153.

Ballard, S.N., 1990, The structural geology of the Little Maria Mountains, Riverside County, California [Ph.D. thesis]: Santa Barbara, University of California, 206 p.

Bartley, J.M., and Glazner, A.F., 1991, En echelon Miocene rifting in the southwestern United States and model for vertical-axis rotation in continental extension: Geology, v. 19, p. 1165–1168, doi: 10.1130/0091-7613(1991)019<1165:EEMRIT>2.3.CO;2.

Bartley, J.M., and Wernicke, B.P., 1984, The Snake Range decollement interpreted as a major extensional shear zone: Tectonics, v. 3, p. 647–657.

Bassett, A.M., and Kupfer, D.H., 1964, A geologic reconnaissance in the southeastern Mojave Desert, California: Special report: California Division of Mines and Geology, v. 83, p. 1–43.

Bennett, R.A., Davis, J.L., and Wernicke, B.P., 1999, Present-day pattern of Cordilleran deformation in the western United States: Geology, v. 27, p. 371–374, doi: 10.1130/0091-7613(1999)027<0371:PDPOCD>2.3.CO;2.

Bennett, R.A., Wernicke, B.P., Niemi, N.A., Friedrich, A.M., and Davis, J.L., 2003, Contemporary strain rates in the northern Basin and Range province from GPS data: Tectonics, v. 22, p. 1008, doi: 10.1029/2001TC001355.

Bird, P., 1998, Kinematic history of the Laramide orogeny in latitudes 35–49 N, western United States: Tectonics, v. 17, p. 780–801, doi: 10.1029/98TC02698.

Bogen, N.L., and Schweickert, R.A., 1985, Magnitude of crustal extension across the northern Basin and Range Province; constraints from paleomagnetism: Earth and Planetary Science Letters, v. 75, no. 1, p. 93–100, doi: 10.1016/0012-821X(85)90054-8.

Bohannon, R.G., and Geist, E., 1998, Upper crustal structure and Neogene tectonic development of the California continental borderland: Geological Society of America Bulletin, v. 110, p. 779–800, doi: 10.1130/0016-7606(1998)110<0779:UCSANT>2.3.CO;2.

Brady, R., Wernicke, B., and Fryxell, J., 2000, Kinematic evolution of a large-offset continental normal fault system, South Virgin Mountains, Nevada: Geological Society of America Bulletin, v. 112, p. 1375–1397, doi: 10.1130/0016-7606(2000)112<1375:KEOALO>2.0.CO;2.

Braun, J., and Pauselli, C., 2004, Tectonic evolution of the Lachlan Fold Belt, southeastern Australia: Constraints from coupled numerical models of crustal deformation and surface erosion driven by subduction of the underlying mantle: Physics of the Earth and Planetary Interiors, v. 141, p. 281–301, doi: 10.1016/j.pepi.2003.11.007.

Burchfiel, B.C., Hodges, K.V., and Royden, L.H., 1987, Geology of Panamint Valley–Saline Valley pull apart system, California: Palinspastic evidence for low-angle geometry of a Neogene range-bounding fault: Journal of Geophysical Research, v. 92, p. 10,422–10,426.

Carr, W.J., Byers, F.M., Jr., and Orkild, P.P., 1986, Stratigraphic and volcano-tectonic relations of Crater Flat Tuff and some older volcanic units, Nye County, Nevada: Reston, Virginia, U.S. Geological Survey, U.S. Geological Survey Professional Paper 1323, 28 p.

Carter, J.N., Luyendyk, B.P., and Terres, R.R., 1987, Neogene clockwise tectonic rotation of the eastern Transverse Ranges, California, suggested by paleomagnetic vectors: Geological Society of America Bulletin, v. 98, p. 199–206, doi: 10.1130/0016-7606(1987)98<199:NCTROT>2.0.CO;2.

Cashman, P.H., and Fontaine, S.A., 2000, Strain partitioning in the northern Walker Lane, western Nevada and northeastern California: Tectonophysics, v. 326, p. 111–130, doi: 10.1016/S0040-1951(00)00149-9.

Cemen, I., Wright, L.A., Drake, R.E., and Johnson, F.C., 1985, Cenozoic sedimentation and sequence of deformational events at the southeastern end of Furnace Creek strike-slip fault-zone, Death Valley region, California, *in* Biddle, K.T., and Christie-Blick, N., eds., Strike-slip deformation, basin formation, and sedimentation: Tulsa, Oklahoma, Society for Sedimentary Geology (SEPM), Society of Economic Paleontologists and Mineralogists Special Publication 37, p. 127–139.

Chapin, C.E., and Cather, S.M., 1994, Tectonic setting of the axial basins of the northern and central Rio Grande rift, *in* Keller, G.R., and Cather, S.M., ed., Basins of the Rio Grande rift: Structure, stratigraphy, and tectonic setting: Geological Society of America Special Paper 291, p. 5–25.

Coney, P.J., 1980, Cordillera metamorphic core complexes: An overview, *in* Crittenden, M.D., Coney, P.J., and Davis, G.H., eds., Cordilleran metamorphic core complexes: Geological Society of America Memoir 153, p. 7–31.

Coogan, J.C., and DeCelles, P.G., 1996, Seismic architecture of the Sevier Desert detachment basin: Evidence for large-scale regional extension: Geology, v. 24, p. 933–936, doi: 10.1130/0091-7613(1996)024<0933:ECATSD>2.3.CO;2.

Coogan, J.C., DeCelles, P.G., Mitra, G., and Sussman, A.J., 1995, New regional balanced cross section across the Sevier Desert region and central Utah thrust belt: Geological Society of America Abstracts with Programs, v. 27, no. 4, p. 7.

Crouch, J.K., and Suppe, J., 1993, Late Cenozoic tectonic evolution of the Los Angeles basin and inner California borderland: A model for core-complex–like crustal extension: Geological Society of America Bulletin, v. 105, p. 1415–1434, doi: 10.1130/0016-7606(1993)105<1415:LCTEOT>2.3.CO;2.

Davis, G.A., 1977, Limitations on displacement and southeastward extent of the Death Valley fault zone, California: Short contributions to California Geology: Special report: California Divisions of Mines and Geology, v. 129, p. 27–33.

Davis, G.A., and Burchfiel, B.C., 1973, Garlock Fault: An intracontinental transform structure, southern California: Geological Society of America Bulletin, v. 84, p. 1407–1422, doi: 10.1130/0016-7606(1973)84<1407:GFAITS>2.0.CO;2.

Davis, G.A., and Lister, G.S., 1988, Detachment faulting in continental extension: Perspectives from the southwestern U.S. Cordillera, *in* Clark, S.P., Jr., Burchfiel, B.C., and Suppe, J., eds., Processes in continental lithospheric deformation: Geological Society of America Special Paper 218, p. 133–159.

Davy, P., Guerin, G., and Brun, J.-P., 1989, Thermal constraints on the tectonic evolution of a metamorphic core complex (Santa Catalina Mountains), Arizona: Earth and Planetary Science Letters, v. 94, p. 425–440, doi: 10.1016/0012-821X(89)90159-3.

Dibblee, T.W., Jr., 1964, Geologic map of the Ord Mountains quadrangle, San Bernardino County, California: U.S. Geological Survey Miscellaneous Geologic Investigations Map I-427, 1 sheet, scale: 1:62,500.

Dibblee, T.W., Jr., 1968, Geologic map of the Twentynine Palms quadrangle, San Bernardino and Riverside counties, California: U.S. Geological Survey Miscellaneous Geologic Investigations Map I-561, 1 sheet, scale: 1:62,500.

Dibblee, T.W., Jr., 1982, Regional geology of the Transverse Ranges Province of southern California, *in* Fife, D., ed., Geology and mineral wealth of the California Transverse ranges: Santa Ana, California: Santa Ana, South Coast Geological Society, Inc., p. 7–26.

Dickinson, W.R., 1991, Tectonic setting of faulted Tertiary strata associated with the Catalina core complex in southern Arizona: Geological Society of America Special Paper 264, p. 106.

Dickinson, W.R., 1996, Kinematics of transrotational tectonism in the California Transverse Ranges and its contribution to cumulative slip along the San Andreas transform fault system: Geological Society of America Special Paper 305, p. 46.

Dickinson, W.R., 2002, The Basin and Range province as a composite extensional domain: International Geology Review, v. 44, no. 1, p. 1–38.

Dickinson, W.R., and Wernicke, B.P., 1997, Reconciliation of San Andreas slip discrepancy by a combination of interior basin-range extension and transrotation near the coast: Geology, v. 25, p. 663–665, doi: 10.1130/0091-7613(1997)025<0663:ROSASD>2.3.CO;2.

Dilles, J.H., and Gans, P.B., 1995, The chronology of Cenozoic volcanism and deformation in the Yerington area, western Basin-and-Range and Walker Lane: Geological Society of America Bulletin, v. 107, p. 474–486, doi: 10.1130/0016-7606(1995)107<0474:TCOCVA>2.3.CO;2.

Dillon, J.T., 1975, Geology of the Chocolate and Cargo Muchacho Mountains, southeasternmost California [Ph.D. thesis]: Santa Barbara, University of California, 405 p.

Dokka, R.K., 1983, Displacements on late Cenozoic strike-slip faults of the central Mojave Desert, California: Geology, v. 11, p. 305–308, doi: 10.1130/0091-7613(1983)11<305:DOLCSF>2.0.CO;2.

Dokka, R.K., 1989, The Mojave extensional belt of southern California: Tectonics, v. 8, p. 363–390.

Dokka, R.K., and Travis, C.J., 1990, Late Cenozoic strike-slip faulting in the Mojave Desert, California: Tectonics, v. 9, no. 2, p. 311–340.

Dokka, R.K., Ross, T.M., and Lu, G., 1998, The Trans Mojave-Sierran shear zone and its role in early Miocene collapse of southwestern North America, *in* Holdsworth, B., Dewey, J., and Strachan, R., eds., Continental transpressional and transtensional tectonics: Geological Society Special Publication 135, p. 183–202.

Duebendorfer, E.M., and Black, R.A., 1992, The kinematic role of transverse structures in continental extension: An example from the Las Vegas Valley shear zone, Nevada: Geology, v. 20, p. 1107–1110, doi: 10.1130/0091-7613(1992)020<1107:KROTSI>2.3.CO;2.

Duebendorfer, E.M., Beard, L.S., and Smith, E.I., 1998, Restoration of Tertiary deformation in the Lake Mead region, southern Nevada; the role of strike-slip transfer faults, *in* Faulds, J.E., and Stewart, J.H., eds., Accommodation zones and transfer zones; the regional segmentation of the Basin and Range province: Geological Society of America Special Paper 323, p. 127–148.

England, P., and Houseman, G., 1986, Finite strain calculations of continental deformation. 2. Comparison with the India-Asia collision zone: Journal of Geophysical Research, v. 91, p. 3664–3676.

England, P., and McKenzie, D., 1982, A thin viscous sheet model for continental deformation: Geophysical Journal of the Royal Astronomical Society, v. 70, p. 295–321.

Faulds, J.E., Henry, C.D., and Hinz, N.H., 2005, Kinematics of the northern Walker Lane; an incipient transform fault along the Pacific-North American Plate boundary: Geology, v. 33, p. 505–508, doi: 10.1130/G21274.1.

Fayon, A.K., Peacock, S.M., Stump, E., and Reynolds Stephen, J., 2000, Fission track analysis of the footwall of the Catalina deatchment fault, Arizona: Tectonic denudation, magmatism and erosion: Journal of Geophysical Research, v. 105, p. 11,047–11,062, doi: 10.1029/1999JB900421.

Fitzgerald, P.G., Fryxell, J.E., and Wernicke, B.P., 1991, Miocene crustal extension and uplift in southeastern Nevada: Constraints from apatite fission track analysis: Geology, v. 19, p. 1013–1016, doi: 10.1130/0091-7613(1991)019<1013:MCEAUI>2.3.CO;2.

Flesch, L.M., Holt, W.E., Haines, A.J., and Shen-Tu, B., 2000, Dynamics of the Pacific–North American plate boundary in the western United States: Science, v. 287, p. 834–836, doi: 10.1126/science.287.5454.834.

Fletcher, J.M., 2003, Tectonic restoration of the Baja California microplate and the geodynamic evolution of the Pacific-North American plate margin: Geological Society of America Abstracts with Programs, v. 35, no. 4, p. 9.

Fletcher, J.M., Bartley, J.M., Martin, M.W., Glazner, A.F., and Walker, J.D., 1995, Large-magnitude continental extension: An example from the central Mojave metamorphic core complex: Geological Society of America Bulletin, v. 107, no. 12, p. 1468–1483, doi: 10.1130/0016-7606(1995)107<1468:LMCEAE>2.3.CO;2.

Foster, D.A., Gleadow, A.J.W., Reynolds, S.J., and Fitzger-

ald, P.G., 1993, Denudation of metamorphic core complexes and the reconstruction of the Transition Zone, west-central Arizona; constraints from apatite fission track thermochronology: Journal of Geophysical Research, v. 98, p. 2167–2185.

Fowler, T.K., Jr., and Calzia, J.P., 1999, Kingston Range detachment fault, southeastern Death Valley region, California; relation to Tertiary deposits and reconstruction of initial dip, *in* Wright, L.A., and Troxel, B.W., eds., Cenozoic basins of the Death Valley region: Geological Society of America Special Paper 333, p. 245–257.

Frei, L.S., 1986, Additional paleomagnetic results from the Sierra Nevada: Further constraints on Basin and Range extension and northward displacement in the western United States: Geological Society of America Bulletin, v. 97, p. 840–849, doi: 10.1130/0016-7606(1986)97<840:APRFTS>2.0.CO;2.

Frei, L.S., Magill, J.R., and Cox, A., 1984, Paleomagnetic results from the central Sierra Nevada: Constraints on reconstructions of the western United States: Tectonics, v. 3, p. 157–177.

Gans, P.B., 1997, Large-magnitude Oligo-Miocene extension in southern Sonora: Implications for the tectonic evolution of northwest Mexico: Tectonics, v. 16, p. 388–408, doi: 10.1029/97TC00496.

Gans, P.B., and Miller, E.L., 1983, Style of mid-Tertiary extension in east-central Nevada: Utah Geology and Mineral Survey Special Studies, v. 59, p. 107–160.

Gans, P.B., Blair, K., MacMillan, I., Wong, M., and Roldan, J., 2003, Structural and magmatic evolution of the Sonoran rifted margin: A preliminary report: Geological Society of America Abstracts with Programs, v. 35, no. 4, p. 21.

Gans, P.B., Miller, E.L., McCarthy, J., and Ouldcott, M.L., 1985, Tertiary extensional faulting and evolving ductile-brittle transition zones in the northern Snake Range and vicinity; new insights from seismic data: Geology, v. 13, p. 189–193, doi: 10.1130/0091-7613(1985)13<189:TEFAED>2.0.CO;2.

Gilder, S., and McNulty, B.A., 1999, Tectonic exhumation and tilting of the Mount Givens pluton, central Sierra Nevada, California: Geology, v. 27, p. 919–922, doi: 10.1130/0091-7613(1999)027<0919:TEATOT>2.3.CO;2.

Glazner, A.F., Bartley, J.M., and Walker, J.D., 1989, Magnitude and significance of Miocene crustal extension in the central Mojave Desert, California: Reply: Geology, v. 17, p. 1061–1062, doi: 10.1130/0091-7613(1989)017<1061:CAROMA>2.3.CO;2.

Glazner, A.F., Walker, J.D., Bartley, J.M., and Fletcher, J.M., 2002, Cenozoic evolution of the Mojave Block of southern California, *in* Glazner, A.F., Walker, J.D., and Bartley, J.M., eds., Geologic evolution of the Mojave Desert and southwestern Basin and Range: Geological Society of America Memoir 195, p. 19–41.

Goodman, E.D., and Malin, P.E., 1992, Evolution of the southern San Joaquin Basin and mid-Tertiary ''transitional'' tectonics, central California: Tectonics, v. 11, p. 478–498.

Graham, S.A., Stanley, R.G., Bent, J.V., and Carter, J.R., 1989, Oligocene and Miocene paleogeography of central California and displacement along the San Andreas fault: Geological Society of America Bulletin, v. 101, p. 711–730, doi: 10.1130/0016-7606(1989)101<0711:OAMPOC>2.3.CO;2.

Guth, P.L., 1989, Day 4. Tertiary extension in the Sheep Range Area, northwestern Clark County, Nevada, *in* Wernicke, B.P., Snow, J.K., Axen, G.J., Burchfiel, B.C., Hodges, K.V., Walker, J.D., and Guth, P.L., eds., Extensional tectonics in the Basin and Range Province between the southern Sierra Nevada and the Colorado Plateau: Washington D.C., Field Trip Guidebook T138, 28th International Geological Congress, American Geophysical Union, p. 33–39.

Hamilton, W.B., 1987, Mesozoic geology and tectonics of the Big Maria Mountains region, southeastern California, *in* Dickinson, W.R., and Klute, M.A., eds., Mesozoic rocks of southern Arizona and adjacent areas: Arizona Geological Society Digest, v. 18, p. 33–47.

Hardyman, R.F., Ekren, E.B., and Proffett, J., 1984, Tertiary tectonics of west-central Nevada—Yerington to Gabbs Valley, Western Geological Excursions, Guidebook, volume 4: Reno, Mackay School of Mines, Department of Geological Sciences, p. 160–231.

Henry, C.D., 1989, Late Cenozoic Basin and Range structure in western Mexico adjacent to the Gulf of California: Geological Society of America Bulletin, v. 101, p. 1147–1156, doi: 10.1130/0016-7606(1989)101<1147:LCBARS>2.3.CO;2.

Henry, C.D., and Aranda-Gomez, J.J., 2000, Plate interactions control middle–late Miocene, proto-Gulf and Basin and Range extension in the southern Basin and Range province: Tectonophysics, v. 318, p. 1–26, doi: 10.1016/S0040-1951(99)00304-2.

Hintze, L.F., 1973, Geologic road logs of western Utah and eastern Nevada: Brigham Young University Research Studies, Geology Series, v. 20, part 2, no.7, 66 p.

Hoisch, T.D., and Simpson, C., 1993, Rise and tilt of metamorphic rocks in the lower plate of a detachment fault in the Funeral Mountains, Death Valley, California: Journal of Geophysical Research, v. 98, no. 4, p. 6805–6827.

Holm, D.K., and Dokka, R.K., 1991, Major late Miocene cooling of the middle crust associated with extensional orogenesis in the Funeral Mountains, California: Geophysical Research Letters, v. 18, no. 9, p. 1775–1778.

Holm, D.K., and Dokka, R.K., 1993, Interpretation and tectonic implications of cooling histories; an example from the Black Mountains, Death Valley extended terrane, California: Earth and Planetary Science Letters, v. 116, no. 1–4, p. 63–80, doi: 10.1016/0012-821X(93)90045-B.

Holm, D.K., Snow, J.K., and Lux, D.R., 1992, Thermal and barometric constraints on the intrusive and unroofing history of the Black Mountains; implications for timing, initial dip, and kinematics of detachment faulting in the Death Valley region, California: Tectonics, v. 11, no. 3, p. 507–522.

Holm, D.K., Geissman, J.W., and Wernicke, B., 1993, Tilt and rotation of the footwall of a major normal fault system: Paleomagnetism of the Black Mountains, Death Valley extended terrane, California: Geological Society of America Bulletin, v. 105, no. 10, p. 1373–1387, doi: 10.1130/0016-7606(1993)105<1373:TAROTF>2.3.CO;2.

Holt, W.E., Chamot-Rooke, N., Le Pichon, X., Haines, A.J., Shen, T.B., and Ren, J., 2000, Velocity field in Asia inferred from Quaternary fault slip rates and global positioning system observations: Journal of Geophysical Research, v. 105, p. 19,185–19,210, doi: 10.1029/2000JB900045.

Hope, R.A., 1966, Geology and structural setting of the eastern Transverse Ranges, southern California [Ph.D. thesis]: Los Angeles, University of California, 201 p.

Hornafius, J.S., Luyendyk, B.P., Terres, R.R., and Kamerling, M.J., 1986, Timing and extent of Neogene tectonic rotation in the western Transverse Ranges, California: Geological Society of America Bulletin, v. 97, p. 1476–1487, doi: 10.1130/0016-7606(1986)97<1476:TAEONT>2.0.CO;2.

Houseman, G., and England, P., 1986, Finite strain calculations of continental deformation. 1. Method and general results for convergent zones: Journal of Geophysical Research, v. 91, p. 3651–3663.

Howard, K.A., and Miller, D.M., 1992, Late Cenozoic faulting at the boundary between the Mojave and Sonoran blocks; Bristol Lake area, California, *in* Richard, S.M., ed., Deformation associated with the Neogene, eastern California shear zone, southeastern California and southwestern Arizona; proceedings: Redlands, California, San Bernardino County Museum Association, San Bernardino County Museum Association Special Publication 92–1, p. 37–47.

Hudson, D.M., and Oriel, W.M., 1979, Geologic map of the Buckskin Range, Nevada, Nevada Bureau of Mines and Geology, no. 64, 1 sheet, scale 1:18,000.

Hudson, M.R., Sawyer, D.A., and Warren, R.G., 1994, Paleomagnetism and rotation constraints for the middle Miocene southwestern Nevada volcanic field: Tectonics, v. 13, no. 2, p. 258–277, doi: 10.1029/93TC03189.

Humphreys, E.D., 1995, Post-Laramide removal of the Farallon slab, western United States: Geology, v. 23, p. 987–990, doi: 10.1130/0091-7613(1995)023<0987:PLROTF>2.3.CO;2.

Humphreys, E.D., Clayton, R.W., and Hager, B.H., 1984, A tomographic image of mantle structure beneath southern California: Geophysical Research Letters, v. 11, no. 7, p. 625–627.

Ingersoll, R.V., 2001, Structural and stratigraphic evolution of the Rio Grande Rift, northern New Mexico and southern Colorado: International Geology Review, v. 43, no. 10, p. 867–891.

Ingersoll, R.V., Devaney, K.A., Geslin, J.K., Cavazza, W., Diamond, D.S., Heins, W.A., Jagiello, K.J., Marsaglia, K.M., Paylor, E.D., II, and Short, P.F., 1996, The Mud Hills, Mojave Desert, California: Structure, stratigraphy, and sedimentology of a rapidly extended terrane: Geological Society of America Special Paper 303, p. 61–84.

Jackson, M., 1991, Paleoseismology of Utah, volume 3: The number and timing of Holocene paleoseismic events on the Nephi and Levan segments, Wasatch fault zone, Utah: Utah Geological Survey Special Study 78, 23 p.

John, B.E., and Foster, D.A., 1993, Structural and thermal constraints on the initiation angle of detachment faulting in the southern Basin and Range: The Chemehuevi Mountains case study: Geological Society of America Bulletin, v. 105, p. 1091–1108, doi: 10.1130/0016-7606(1993)105<1091:SATCOT>2.3.CO;2.

Lavier, L.L., and Buck, W.R., 2002, Half graben versus large-offset low-angle normal fault: Importance of keeping cool during normal faulting: Journal of Geophysical Research, v. 107, p. 2122, doi: 10.1029/2001JB000513.

Lee, J., 1995, Rapid uplift and rotation of mylonitic rocks from beneath a detachment fault: Insights from potassium feldspar $^{40}Ar/^{39}Ar$ thermochronology, northern Snake Range, Nevada: Tectonics, v. 14, p. 54–77, doi: 10.1029/94TC01508.

Lee, J., Miller, M.M., Crippen, R., Hacker, B., and Ledesma Vazquez, J., 1996, Middle Miocene extension in the Gulf Extensional Province, Baja California: Evidence from the southern Sierra Juarez: Geological Society of America Bulletin, v. 108, p. 505–525, doi: 10.1130/0016-7606(1996)108<0505:MMEITG>2.3.CO;2.

Lewis, C.J., Wernicke, B.P., Selverstone, J., and Bartley, J.M., 1999, Deep burial of the footwall of the northern Snake Range decollement, Nevada: Geological Society of America Bulletin, v. 111, p. 39–51, doi: 10.1130/0016-7606(1999)111<0039:DBOTFO>2.3.CO;2.

Long, K.B., Baldwin, S.L., and Gehrels, G.E., 1995, Tectonothermal evolution of the Pinaleno-Jackson Mountain core complex, southeast Arizona: Geological Society of America Bulletin, v. 107, p. 1231–1240, doi: 10.1130/0016-7606(1995)107<1231:TEOTPO>2.3.CO;2.

Lund, K., Beard, S.L., and Perry, W.J., 1993, Relation between extensional geometry of the northern Grant Range and oil occurrences in Railroad Valley, east-central Nevada: AAPG Bulletin, v. 77, p. 945–962.

Luyendyk, B.P., 1991, A model for Neogene crustal rotations, transtension, and transpression in southern California: Geological Society of America Bulletin, v. 103, p. 1528–1536, doi: 10.1130/0016-7606(1991)103<1528:AMFNCR>2.3.CO;2.

Machette, M.N., Personius, S.F., and Nelson, A.R., 1992, Paleoseismology of the Wasatch fault zone; a summary of recent investigations, interpretations, and conclusions, *in* Gori, P.L., and Hays, W.W., eds., Assessment of regional earthquake hazards and risk along the Wasatch Front, Utah:U.S. Geological Survey Professional Paper, v. 1500-A, p. A1–A71.

Martin, M.W., Glazner, A.F., Walker, J.D., and Schermer, E.R., 1993, Evidence for right-lateral transfer faulting accommodating en echelon Miocene extension, Mojave Desert, California: Geology, v. 21, p. 355–358, doi: 10.1130/0091-7613(1993)021<0355:EFRLTF>2.3.CO;2.

Matthews, V., III, 1976, Correlation of Pinnacles and Neenach volcanic formations and their bearing on the San Andreas problem: American Association of Petroleum Geologists Bulletin, v. 51, p. 2128–2141.

McClusky, S.S., Bjornstad, S., Hager, B., King, R., Meade, B., Miller, M., Monastero, F., and Souter, B., 2001, Present-day kinematics of the Eastern California Shear Zone from a geodetically constrained block model: Geophysical Research Letters, v. 28, p. 3369–3372, doi: 10.1029/2001GL013091.

McQuarrie, N., Stock, J.M., Verdel, C., and Wernicke, B.P., 2003, Cenozoic evolution of Neotethys and implications for the causes of plate motions: Geophysical Research Letters, v. 30, p. 2036, doi: 10.1029/2003GL017992.

McWilliams, M.O., and Li, Y., 1985, Oroclinal folding of the southern Sierra Nevada batholith: Science, v. 230, p. 172–175.

Miller, D.M., and Yount, J.C., 2002, Late Cenozoic tectonic evolution of the north-central Mojave Desert inferred from fault history and physiographic evolution of the Fort Irwin area, *in* Glazner, A.F., Walker, J.D., and Bartley, J.M., eds., Geologic evolution of the Mojave Desert and southwestern Basin and Range: Geological Society of America Memoir 195, p. 173–198.

Miller, E.L., Gans, P.B., and Garing, J., 1983, The Snake Range decollement: An exhumed mid-Tertiary ductile-brittle transition: Tectonics, v. 2, p. 239–263.

Miller, E.L., Dumitru, T.A., Brown, R.W., and Gans, P.B., 1999, Rapid Miocene slip on the Snake Range–Deep Creek Range fault system, east-central Nevada: Geological Society of America Bulletin, v. 111, no. 6, p. 886–905, doi: 10.1130/0016-7606(1999)111<0886:RMSOTS>2.3.CO;2.

Miller, F.K., and Morton, D.M., 1980, Potassium-argon geochronology of the eastern Transverse Ranges and southern Mojave Desert, southern California, U.S.: Reston, Virginia, U.S. Geological Survey, Geological Survey Professional Paper 1152, 30 p.

Miller, M., Johnson, D., Dixon, T., and Dokka, R.K., 2001, Refined kinematics of the eastern California shear zone from GPS observations, 1993–1998: Journal of Geophysical Research, v. 106, p. 2245–2263, doi: 10.1029/2000JB900328.

Namson, J.S., and Davis, T.L., 1988a, Structural transect of the western Transverse Ranges, California: Implications for lithospheric kinematics and seismic risk evaluation: Geology, v. 16, p. 675–679, doi: 10.1130/0091-7613(1988)016<0675:STOTWT>2.3.CO;2.

Namson, J.S., and Davis, T.L., 1988b, Seismically active fold-thrust belt in the San Joaquin Valley, central California: Geological Society of America Bulletin, v. 100, p. 257–273, doi: 10.1130/0016-7606(1988)100<0257:SAFATB>2.3.CO;2.

Namson, J.S., and Davis, T.L., 1990, Late Cenozoic fold and thrust belt of the southern Coast Ranges and Santa Maria Basin, California: American Association of Petroleum Geologists Bulletin, v. 74, p. 467–492.

Niemi, N.A., 2002, Extensional tectonics in the Basin and Range Province and the geology of the Grapevine Mountains, Death Valley Region, California and Nevada [Ph.D. thesis]: Pasadena, California, California Institute of Technology, 344 p.

Niemi, N.A., Wernicke, B.P., Brady, R.J., Saleeby, J.B., and Dunne, G.C., 2001, Distribution and provenance of the middle Miocene Eagle Mountain Formation, and implications for regional kinematic analysis of the Basin and Range province: Geological Society of America Bulletin, v. 113, p. 419–442, doi: 10.1130/0016-7606(2001)113<0419:DAPOTM>2.0.CO;2.

Niemi, N.A., Wernicke, B.P., Friedrich, A.M., Simons, M., Bennett, R.A., and Davis, J.L., 2004, BARGEN continuous GPS data across the eastern Basin and Range province, and implications for fault system dynamics: Geophysical Journal International, v. 159, p. 842–862, doi: 10.1111/j.1365-246X.2004.02454.x.

Nourse, J.A., Anderson, T.H., and Silver, L.T., 1994, Tertiary metamorphic core complexes in Sonora, northwestern Mexico: Tectonics, v. 13, p. 1161–1182, doi: 10.1029/93TC03324.

Oskin, M., and Stock, J., 2003, Pacific-North America plate motion and opening of the Upper Delfín basin, northern Gulf of California, Mexico: Geological Society of America Bulletin, v. 115, no. 10, p. 1173–1190, doi: 10.1130/B25154.1.

Oskin, M., and Iriondo, A., 2004, Large magnitude transient strain accumulation on the Blackwater fault, Eastern California shear zone: Geology, v. 32, p. 313–316, doi: 10.1130/G20223.1.

Oskin, M., Stock, J., and Martin-Barajas, A., 2001, Rapid localization of Pacific–North America plate motion in the Gulf of California: Geology, v. 29, p. 459–462, doi: 10.1130/0091-7613(2001)029<0459:RLOPNA>2.0.CO;2.

Page, B.M., Thompson, G.A., and Coleman, R.G., 1998, Late Cenozoic tectonics of the central and southern ranges of California: Geological Society of America Bulletin, v. 110, p. 846–876, doi: 10.1130/0016-7606(1998)110<0846:OLCTOT>2.3.CO;2.

Plescia, J.B., and Calderone, G.J., 1986, Paleomagnetic constraints on the timing and extent of rotation of the Tehachapi Mountains, California: Geological Society of America Abstracts with Programs, v. 18, p. 171.

Powell, R.E., 1981, Geology of the crystalline basement complex, eastern Transverse Ranges, southern California: Constraints on regional tectonic interpretation [Ph.D. thesis]: Pasadena, California, California Institute of Technology, 441 p.

Reheis, M.C., 1993, Neogene tectonism from the southwestern Nevada volcanic field to the White Mountains, California; part II, Late Cenozoic history of the southern Fish Lake Valley fault zone, Nevada and California, *in* Lahren, M.M., Trexle, J.H., Jr., and Spinosa, C., eds., Crustal evolution of the Great Basin and the Sierra Nevada: Reno, University of Nevada, p. 370–382.

Reheis, M.C., and Sawyer, T.L., 1997, Late Cenozoic history and slip rates of the Fish Lake Valley, Emigrant Peak, and Deep Springs fault zones, Nevada and California: Geological Society of America Bulletin, v. 109, no. 3, p. 280–299, doi: 10.1130/0016-7606(1997)109<0280:LCHASR>2.3.CO;2.

Reynolds, S.J., 1985, Geology of the South Mountains, central Arizona: Arizona Bureau of Geology and Mineral Technology Bulletin, v. 195, 61 p.

Richard, S.M., 1993, Palinspastic reconstruction of southeastern California and southwestern Arizona for the middle Miocene: Tectonics, v. 12, p. 830–854.

Richard, S.M., and Dokka, R.K., 1992, Geology of the Packard Well fault zone, southeastern California, *in* Richard, S.M., ed., Deformation associated with the Neogene, eastern California shear zone, southeastern California and southwestern Arizona; proceedings: Redlands, California, San Bernardino County Museum Association, San Bernardino County Museum Association Special Publication 92–1, p. 71–74.

Richard, S.M., Fryxell, J.E., and Sutter, J.F., 1990, Tertiary structure and thermal history of the Harquahala and Buckskin Mountains, west central Arizona: Implications for denudation by a major detachment fault system: Journal of Geophysical Research, v. 95, p. 19,973–19,987.

Richard, S.M., Sherrod, D.R., and Tosdal, R.M., 1992, Cibola Pass fault, southwestern Arizona, *in* Richard, S.M., ed., Deformation associated with the Neogene, eastern California shear zone, southeastern California and southwestern Arizona; proceedings: Redlands, California, San Bernardino County Museum Association, San Bernardino County Museum Association Special Publication 92–1, p. 66–70.

Ron, H., and Nur, A., 1996, Vertical axis rotation in the Mojave: Evidence from the Independence dike swarm: Geology, v. 24, no. 11, p. 973–976, doi: 10.1130/0091-7613(1996)024<0973:VARITM>2.3.CO.

Rotstein, Y., Combs, J., and Biehler, S., 1976, Gravity investigation in the southern Mojave Desert, California: Geological Society of America Bulletin, v. 87, p. 981–993, doi: 10.1130/0016-7606(1976)87<981:GIITSM>2.0.CO;2.

Russell, L.R., and Snelson, S., 1994, Structure and tectonics of the Albuquerque Basin segment of the Rio Grande Rift; insights from reflection seismic data, *in* Keller, G.R., and Cather, S.M., eds., Basins of the Rio Grande Rift: Structure, stratigraphy, and tectonic setting: Geological Society of America Special Paper 291, p. 83–112.

Sauber, J., Thatcher, W., Solomon, S., and Lisowski, M., 1994, Geodetic slip rate for the eastern California shear zone and the recurrence time of Mojave desert earthquakes: Nature, v. 367, p. 264–266, doi: 10.1038/367264a0.

Savage, J.C., Lisowski, M., and Prescott, W., 1990, An apparent shear zone trending north-northwest across the Mojave Desert into Owens Valley, eastern California: Geophysical Research Letters, v. 17, p. 2113–2116.

Schermer, E.R., Luyendyk, B.P., and Cisowski, S., 1996, Late Cenozoic structure and tectonics of the northern Mojave Desert: Tectonics, v. 15, no. 5, p. 905–932, doi: 10.1029/96TC00131.

Scott, R.J., Foster, D.A., and Lister, G.S., 1998, Tectonic implications of rapid cooling of lower plate rocks from the Buckskin-Rawhide metamorphic core complex, west-central Arizona: Geological Society of America Bulletin, v. 110, p. 588–614, doi: 10.1130/0016-7606(1998)110<0588:TIORCO>2.3.CO;2.

Sieh, K., and Jahns, R.H., 1984, Holocene activity of the San Andreas fault at Wallace Creek, California: Geological Society of America Bulletin, v. 95, p. 883–896, doi: 10.1130/0016-7606(1984)95<883:HAOTSA>2.0.CO;2.

Smith, D.L., 1992, History and kinematics of Cenozoic extension in the northern Toiyabe Range, Lander County, Nevada: Geological Society of America Bulletin, v. 104, p. 789–801, doi: 10.1130/0016-7606(1992)104<0789:HAKOCE>2.3.CO;2.

Smith, D.L., Gans, P.B., and Miller, E.L., 1991, Palinspastic restoration of Cenozoic extension in the central and eastern Basin and Range Province at latitude 39–40 degrees N, *in* Raines, G.L., Lisle, R.E., Schafer, R.W., and Wilkinson, W.H., eds., Geology and ore deposits of the Great Basin; symposium proceedings: Reno, Nevada, Geological Society of Nevada, p. 75–86.

Smith, R.B., and Bruhn, R.L., 1984, Intraplate extensional tectonics of the western U.S. Cordillera—Inferences on structural style from seismic-reflection data, regional tectonics and thermal-mechanical models of brittle ductile deformation: Journal of Geophysical Research, v. 89, p. 5733–5762.

Snow, J.K., 1992, Large-magnitude Permian shortening and continental margin tectonics in the southern Cordillera: Geological Society of America Bulletin, v. 104, no. 1, p. 80–105, doi: 10.1130/0016-7606(1992)104<0080:LMPSAC>2.3.CO;2.

Snow, J.K., and Lux, D.R., 1999, Tectono-sequence stratigraphy of Tertiary rocks in the Cottonwood Mountains and northern Death Valley area, California and Nevada, *in* Wright, L.A., and Troxel, B.W., eds., Cenozoic basins of the Death Valley region: Geological Society of America Special Paper 333, p. 17–64.

Snow, J.K., and Prave, A.R., 1994, Covariance of structural and stratigraphic trends; evidence for anticlockwise rotation within the Walker Lane Belt, Death Valley region, California and Nevada: Tectonics, v. 13, no. 3, p. 712–724, doi: 10.1029/93TC02943.

Snow, J.K., and Wernicke, B.P., 1989, Uniqueness of geological correlations; an example from the Death Valley extended terrain: Geological Society of America Bulletin, v. 101, no. 11, p. 1351–1362, doi: 10.1130/0016-7606(1989)101<1351:UOGCAE>2.3.CO;2.

Snow, J.K., and Wernicke, B.P., 2000, Cenozoic tectonism in the central Basin and Range: Magnitude, rate and distribution of upper crustal strain: American Journal of Science, v. 300, p. 659–719.

Spencer, J.E., and Reynolds, S.J., 1989, Middle Tertiary tectonics of Arizona and adjacent areas, *in* Jenney, J.P., and Reynolds, S.J., eds., Geologic evolution of Arizona: Tucson, Arizona, Arizona Geological Society, Arizona Geological Society Digest, v. 17, p. 539–574.

Spencer, J.E., and Reynolds, S.J., 1991, Tectonics of mid-Tertiary extension along a transect through west-central Arizona: Tectonics, v. 10, no. 6, p. 1024–1221.

Spencer, J.E., Richard, S.M., Reynolds, S.J., Miller, R.J., Shafiqullah, M., Gilbert, W.G., and Grubensky, M.J., 1995, Spatial and temporal relationships between mid-Tertiary magnetism and extension in southwestern Arizona: Journal of Geophysical Research, Solid Earth and Planets, v. 100, no. B6, p. 10,321–10,351, doi: 10.1029/94JB02817.

Stock, J.M., and Hodges, K.V., 1989, Pre-Pliocene extension around the Gulf of California and the transfer of

Baja California to the Pacific Plate: Tectonics, v. 8, p. 99–115.

Stockli, D.F., 1999, Regional timing and spatial distribution of Miocene extension in the northern Basin and Range Province [Ph.D. thesis]: Stanford, California, Stanford University, 239 p.

Stockli, D.F., Linn, J.K., Walker, J.D., and Dumitru, T.A., 2001, Miocene unroofing of the Canyon Range during extension along the Sevier Desert Detachment, west-central Utah: Tectonics, v. 20, p. 289–307, doi: 10.1029/2000TC001237.

Stockli, D. F., Surpless, B.E., Dumitru, T.A., and Farley, K.A., 2002, Thermochronological constraints on the timing and magnitude of Miocene and Pliocene extension in the central Wassuk Range, western Nevada: Tectonics, v. 21, no. 4, p. 10-1–10-17, doi: 10.1029/2001TC001295.

Stone, P., and Pelka, G.J., 1989, Geologic map of the Palen–McCoy Wilderness study area and vicinity: Riverside County, California, Geological Survey Miscellaneous Field Investigations Map MF-2070, 1 sheet, scale: 1:62,500.

Surpless, B., 1999, Tectonic evolution of the Sierra Nevada–Basin and Range transition zone: A study of crustal evolution in extensional provinces [Ph.D. thesis]: Stanford, California, Stanford University, 186 p.

Taylor, W.J., Bartley, J.M., Lux, D.R., and Axen, G.J., 1989, Timing of Tertiary extension in the Railroad Valley–Pioche Transect, Nevada: Constraints from $^{40}Ar/^{39}Ar$ ages of volcanic rocks: Journal of Geophysical Research, v. 94, p. 7757–7774.

Tennyson, M.E., 1989, Pre-transform early Miocene extension in western California: Geology, v. 17, p. 792–796, doi: 10.1130/0091-7613(1989)017<0792:PTEMEI>2.3.CO;2.

Walker, J.D., Bartley, J.M., and Glazner, A.F., 1990, Large-magnitude Miocene extension in the central Mojave Desert; implications for Paleozoic to Tertiary paleogeography and tectonics: Journal of Geophysical Research, v. 95, p. 557–569.

Walker, J.D., Fletcher, J.M., Fillmore, R.P., Martin, M.W., Taylor, W.J., Glazner, A.F., and Bartley, J.M., 1995, Connection between igneous activity and extension in the central Mojave metamorphic core complex, California: Journal of Geophysical Research, v. 100, p. 10,477–10,494, doi: 10.1029/94JB03132.

Wernicke, B., 1992, Cenozoic extensional tectonics of the U.S. Cordillera, *in* Burchfiel, B.C., Lipman, P.W., and Zoback, M.L., eds., The Cordilleran Orogen: Conterminous U.S.: Boulder, Colorado, Geological Society of America, The Geology of North America, v. G-3, p. 553–581.

Wernicke, B., and Snow, J.K., 1998, Cenozoic tectonism in the central Basin and Range: Motion of the Sierran–Great Valley Block: International Geology Review, v. 40, p. 403–410.

Wernicke, B., Axen, G.J., and Snow, J.K., 1988, Basin and Range extensional tectonics at the latitude of Las Vegas, Nevada: Geological Society of America Bulletin, v. 100, p. 1738–1757, doi: 10.1130/0016-7606(1988)100<1738:BARETA>2.3.CO;2.

Wills, S., Anders, M.H., and Christie-Blick, N., 2005, Pattern of Mesozoic thrust surfaces and Tertiary normal faults in the Sevier Desert subsurface, west-central Utah: American Journal of Science, v. 305, p. 42–100.

Manuscript Received by the Society 5 April 2005
Revised Manuscript Received 29 August 2005
Manuscript Accepted 23 September 2005

Printed in the USA